KSME

Springer

Journal of Mechanical Science and Technology 35 (3) 2021

Invited Review Article
DOI 10.1007/s12206-021-0243-7

Keywords:
· Advanced nanofabrication technique
· Nanogap fabrication
· Nanostructure fabrication
· Single-digit-nanometer
· Sub-10 nm
· Nanophotonic devices

Correspondence to:
Junsuk Rho
jsrho@postech.ac.kr

[#] These authors equally contributed to this work as first author.

Citation:
Oh, D. K., Jeong, H., Kim, J., Kim, Y., Kim, I., Ok, J. G., Rho, J. (2021). Top-down nanofabrication approaches toward single-digit-nanometer scale structures. Journal of Mechanical Science and Technology 35 (3) (2021) 837~859.
http://doi.org/10.1007/s12206-021-0243-7

Received December 21st, 2020
Revised January 21st, 2021
Accepted January 27th, 2021

† Recommended by Editor Chang-Soo Han

© The Korean Society of Mechanical Engineers and Springer-Verlag GmbH Germany, part of Springer Nature 2021

Top-down nanofabrication approaches toward single-digit-nanometer scale structures

Dong Kyo Oh[1,#], Heonyeong Jeong[1,#], Joohoon Kim[1,#], Yeseul Kim[1,#], Inki Kim[1], Jong G. Ok[2] and Junsuk Rho[1,3]

[1]Department of Mechanical Engineering, Pohang University of Science and Technology (POSTECH), Pohang 37673, Korea, [2]Department of Mechanical and Automotive Engineering, Seoul National University of Science and Technology, Seoul 01811, Korea, [3]Department of Chemical Engineering, Pohang University of Science and Technology (POSTECH), Pohang 37673, Korea

Abstract Sub-10 nm nanostructures have received broad interest for their intriguing nano-optical phenomena, such as extreme field localization and enhancement, quantum tunneling effect, and strong coupling. The range of cutting-edge applications based on single-digit-nanometer scale structures has expanded with the development of nanofabrication technologies. However, challenges still remain in overcoming fabrication limits, such as scalability, controllability, and reproducibility for further practical applications of the sub-10 nm nanostructures. In this review, we discuss the recent advances in top-down nanofabrication methods towards single-digit-nanometer-sized structures. The well-known examples include electron beam lithography (EBL), focused ion beam (FIB) milling or lithography, atomic layer deposition (ALD), and other unconventional techniques to obtain sub-10 nm nanostructures or nanogaps. We discuss state-of-the-art applications for sub-10 nm nanophotonics such as optical trapping or sensing devices, imaging devices, and electronic devices.

1. Introduction

Nanoscale patterns have been fabricated for practical applications such as transistors [1-6], displays [7-17], optical devices [18-25], absorbers [26-32] tunable color filters [33-37], and other functional devices [38-50] because of their unique mechanical and/or optical properties which are not realized in bulky sizes. Especially, metasurfaces of sub-100 nm nanostructures which are applied for controlling light have been mainly produced by electron beam lithography (EBL) [8, 51-56] and focused ion beam (FIB) milling [48, 57-60]. High throughput fabrication of these optical nanostructures is being actively studied, combined with alternative nanopatterning processes such as nanoimprint lithography (NIL) [61-65], selective deposition [66-68], and direct laser patterning [69-71].

Moreover, sub-10 nm nanostructures are being researched actively due to their distinctive phenomena at the sub-10 nm scale such as plasmonic-coupled electromagnetic field localization and enhancement [18, 72, 73], quantum tunneling effect [74-77], and strong coupling [78-80]. These properties have been applied to promising optical devices such as optical trapping [19, 20, 81, 82], spectroscopy [80, 83-88], sensing [20, 89, 90], electrical trapping [91, 92], memory devices [38], and biomolecule identification [76, 93]. However, conventional top-down technologies such as EBL and FIB that are widely used to fabricate nanostructures have a resolution limit [94-97], preventing progress toward a next-generation nanofabrication method. Therefore, to solve the drawbacks, overcoming the resolution limit of EBL and FIB technologies or alternative nanofabrication methods based on a top-down process are needed.

In this review, we mainly focus on the progress of top-down approaches for sub-10 nm fabrication. First, we discuss advanced technologies of EBL and FIB. Afterward, we describe the development of the ALD process suitable for single-digit resolution. Then, we discuss unconventional nanofabrication methods such as NIL, structure collapsing, scanning probe lithogra-

 DOI 10.1007/s12206-021-0243-7

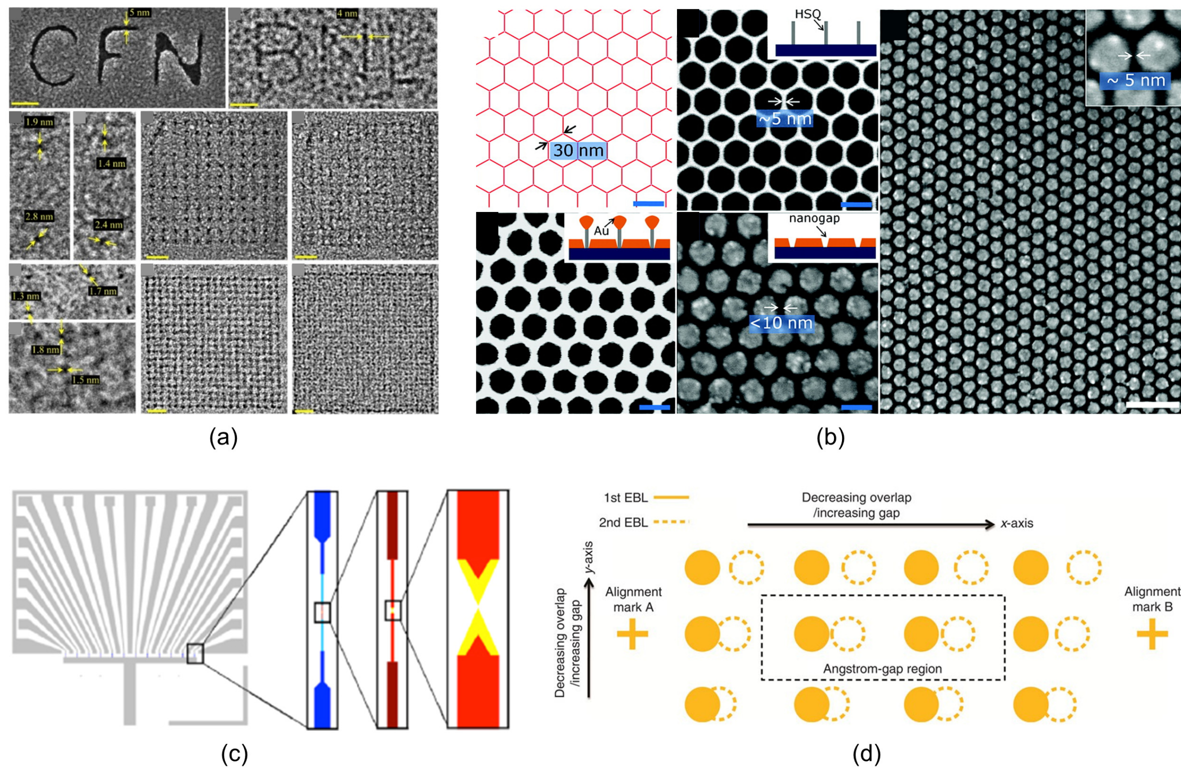

Fig. 1. EBL for fabricating sub-10 nm nanostructures: (a) SEM images of sub-10 nm line patterns and nanohole arrays using AC-EBL [104]; (b) schematic and SEM images of sub-10 nm hexagonal nanogap fabrication using HSQ [106]; (c) schematic of sub-10 nm nanogap fabrication using EBL proximity effect correction [109]; (d) schematic of sub-1 nm nanogap using EBL overlay technique [111] (adapted with permission from Fig. 1 in Refs. [104, 106, 109, 111]).

phy (SPL), and pattern cracking in the views of fabrication for sub-10 nm nanostructures and nanogaps. Next, we introduce state-of-the-art sub-10 nm plasmonic applications such as optical sensing/trapping, imaging, and electronic devices. Finally, we review each of the processes and discuss outlooks toward practical applications of these emerging nanofabrication methods.

2. Electron beam lithography

EBL is a widely used process for several tens nanometer fabrication [98, 99], so EBL can be used for the sub-10 nm fabrication. Using various pattern transfer methods such as lift-off and etching [100], it is possible to create sub-100 nm two-dimensional (2D) to three-dimensional (3D) structures through an overlay technique [101]. However, it is difficult to fabricate sub-10 nm patterns with general EBL because of the limited resolution due to a 2-10 nm electron beam size and the proximity effect [102]. The electron beam size is much larger than the electron diffraction limit of 0.007 nm at 30 kV [103]. Therefore, to overcome the resolution limit due to the beam size, sub-10 nm fabrication methods have been developed using advanced techniques such as aberration-corrected EBL (AC-EBL) [102, 104, 105], negative resists with high resolution [106-108], proximity effect correction [3, 109, 110], and others [111-113].

The main factors that degrade the resolution in the EBL can be classified into four categories: (1) the electron beam size by equipment limitation of beam controllers such as magnetic lenses and beam deflectors [103], (2) the interaction between the electron beam and resist during exposure, (3) the pattern distortion by the resist development, and (4) the distortion in the pattern transfer process [104]. AC-EBL can overcome limitations (1) and (2), while negative resists with high resolution and proximity effect correction can be used to solve limitations (3) and (4).

2.1 Aberration-corrected electron beam lithography

AC-EBL has been studied as a sub-10 nm fabrication method utilizing the existing EBL fabrication process. Scanning electron microscopes (SEM) correct aberration by detecting the reflected electrons of the secondary electrons (SE) and backscattered electrons (BSE) from the substrate, while scanning transmission electron microscopes (STEM) can also detect transmitted electrons through the ADF detector and correct more aberration [114]. AC-EBL uses the precise detecting principle applied to STEM for enhancing aberration correction [102, 104, 105], so has a smaller electron beam size and prevents the resolution degrading factors (1) and (2). AC-EBL enables the fabrication of sub-10 nm nanostructures as shown in Fig. 1(a). Since the fabrication process of AC-EBL is similar to existing EBL, it has advantages such as a wide selection of

materials and intricate patterning.

2.2 High-resolution of negative resist

Hydrogen silsesquioxane (HSQ) has been used as a negative resist with high resolution to fabricate sub-10 nm nanostructures by solving the resolution degrading factor (3) [106-108]. EBL patterning by HSQ can have a 2 nm minimum feature size in the commonly used electron beam resists such as poly(methyl methacrylate) (PMMA), ZEP520, SU-8, and HSQ, etc. [115]. When HSQ is salty developed, the resist contrast is considerably improved, so whether the exposed resist has a chemical change is determined depending on whether it is more or less than the appropriate dose [108, 116]. Only the portion of HSQ exposed with the electron beam is developed, achieving high resolution of nanostructures. Therefore, it is possible to fabricate sub-10 nm nanopatterns with a wide selection of materials like existing EBL using HSQ. In addition, HSQ can be used with AC-EBL to solve the resolution limitations (1~3) of EBL [104]. Fig. 1(b) shows a schematic of fabricating a sub-10 nm nanogap using HSQ. The top left panel is a CAD file showing the scanned area, which is imported into the EBL equipment to expose the shape. The top center panel shows the developed pattern of the exposed HSQ and a 5 nm-thick hexagonal wall. The bottom left panel shows gold (Au) deposition on HSQ. The last two panels show that the lift-off succeeded in forming a sub-10 nm nanogap. The Au particles agglomerate on the HSQ, creating a nanogap slightly wider than the sidewall thickness. If a positive resist is used to create such a sub-10 nm nanogap, since the exposure area is larger than negative resist, the proximity effect is greater, and therefore the resolution is lower.

Using the high etch resistance of HSQ, sub-10 nm pattern transfer is possible through HSQ mask etching [107, 117-119]. The silicon (Si) substrate was etched using a sub-10 nm HSQ pattern fabricated using EBL as an etch mask [117]. The high etch resistance of HSQ allowed Si substrate to be etched to a 50:1 aspect ratio, resulting in sub-10 nm Si nanowires. The PMMA/HSQ double layer resist enabled sub-10 nm etching nanofabrication without hydrofluoric acid (HF) [118]. When HSQ is used for etching, the HSQ mask should be erased with HF, and HF removes oxides such as glass. In this research, PMMA/HSQ double layer resist was spin-coated, HSQ pattern fabricated by EBL was used to etch PMMA, and then sub-10 nm Au nanopattern was created through lift-off process. Sub-10 nm germanium (Ge) pattern was fabricated using HSQ [107]. It is difficult to create Ge patterns with high resolution despite using HSQ because Ge oxides are formed and it collides with the developed pattern during the water cleaning process. In this research, a high resolution process was shown by removing native Ge oxides using acid.

2.3 Proximity effect correction

As a method to reduce the distortion by development and the pattern transfer process, proximity effect correction has been studied for fabricating sub-10 nm nanostructures [3, 109, 110] as in Fig. 1(c). Since the electron is scattered into the incident position of the substrate, the exposed pattern is developed with distortion unlike the area scanned by the electron beam, a phenomenon called the proximity effect. If the EBL is carried out under the same conditions, the proximity effect occurs almost the same, so it is possible to fabricate a sub-10 nm nanogap by calculating the size of the pattern increase. Using a developed area wider than the scan area, narrowing the gap between two objects is possible such as a bow-tie nanogap [110]. However, the proximity effect mainly occurs in the direction of expanding the pattern, so this method is difficult to fabricate sub-10 nm grating or nanodots contrary to nanogap [120, 121].

2.4 Others

In addition, other methods of achieving sub-10 nm fabrication such as resist heating, pattern transfer with high resolution, and multiple exposure have been researched [111-113]. Homogeneous PMMA resist layers were formed through a thermal process to reduce the surface roughness, thereby fabricating sub-5 nm nanohole arrays [112]. Sub-10 nm nanogaps were fabricated using a free-standing 10 nm wide mesh pattern of double-layered HSQ/PMMA [113]. This method solves limitation (4) enabling extreme undercut development. However, large-area fabrication is difficult because the area between the supports is small. Sub-10 nm nanogaps were fabricated by closing two nanoparticles (NPs) as much as possible with an overlay [111]. As in Fig. 1(d), the first EBL arranges a number of nanoparticles at regular intervals. After that, the second NPs are fabricated by varying the interval from -10 to 10 nm from the first NPs. Because alignment errors occur during the overlay process, sub-10 nm gaps of NPs can be chosen after the actual fabrication. However, it is difficult to use this method for mass manufacturing since the sub-10 nm nanogaps are fabricated by accident.

3. Focused ion beam

Sub-10 nm FIB fabrication has been researched in the direction of using a high resolution light ion beam or overcoming the resolution limit of gallium (Ga) ion beam. In general, FIB fabrication uses Ga ion beams generated by a liquid metal ion source (LMIS). However, since it has a resolution limit of about 5 nm [122] and the scattered Ga ions destroy the surroundings, it is difficult to practically fabricate sub-10 nm features. To solve this problem, a light ion beam was developed based on a gas field ion source (GFIS), which uses stable inert gases such as helium (He) and neon (Ne). The ion beam size is approximately 1.9 and 0.5 nm for Ne and He ion beams [57], respectively, which is high enough to fabricate sub-10 nm features considering ions scattering into the substrate. To overcome the limitations of Ga ion beam, proximity effect correction [60, 123]

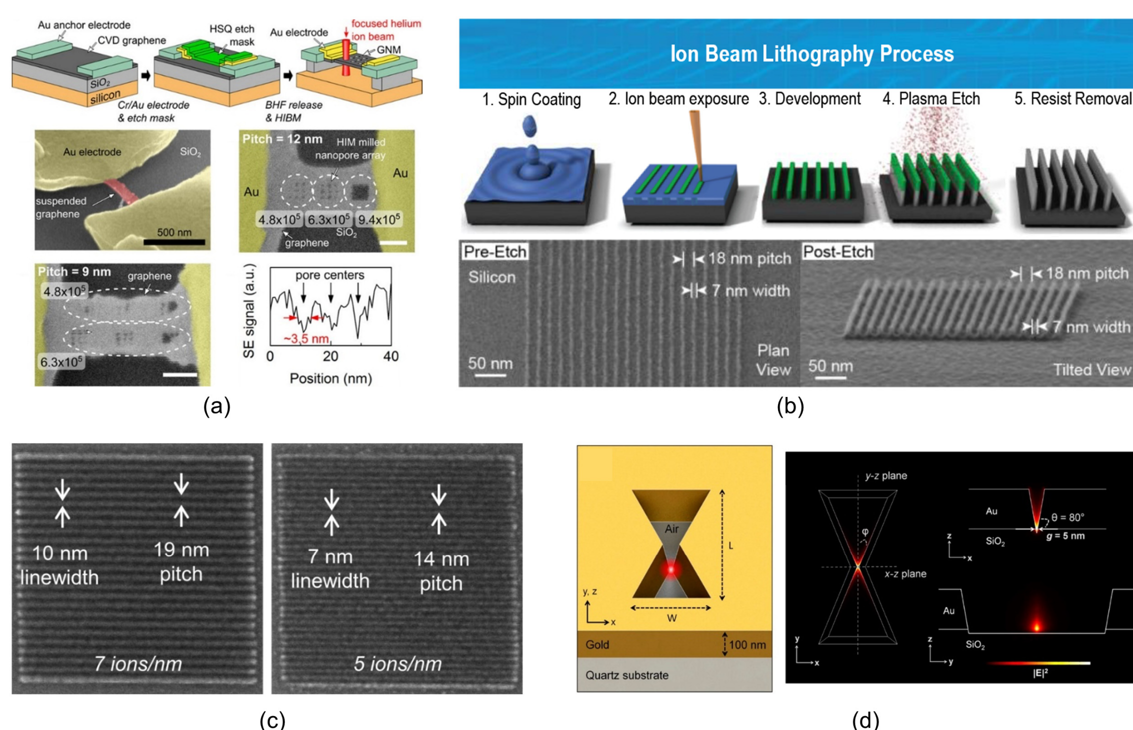

Fig. 2. FIB for fabricating sub-10 nm nanostructures: (a) schematic of graphene nanomesh using EBL with SiO_2 etching, and SEM images for FIB milling process [125]; (b) fabrication process of ion beam lithography and SEM images of 7 nm width Si grating fabricated by HIBL [134]; (c) SEM images of 7 nm linewidth grating fabricated by NIBL [59]; (d) hole-type Au bow tie for capturing photons which is fabricated by GIBM with proximity effect correction [60] (adapted with permission from Fig. 2 in Refs. [59, 60, 125, 134]).

and breaking grain boundary [124] have been studied. They are a solution to low resolution of the Ga ion beam.

3.1 Helium ion beam

For high resolution FIB milling and lithography, Ne and He ions are essential because of their atomic weight and chemical properties. In FIB milling, an ion beam irradiated on the surface physically scrapes the sample to create a desired shape. Since the size of the ion beam directly affects the resolution, it is possible to easily mill sub-10 nm features by using a light ion beam with a small beam spot size. In FIB lithography, an ion beam causes a chemical change in an irradiated resist to create the resist patterns, and then a pattern transfer process such as lift-off or etching is needed. In the resist-based nanofabrication, a small beam size can have high resolution like EBL. In addition, sub-10 nm fabrication is mainly used in electronics, optics, and chemistry, so inactive ions implanted into the sample have the least influence on electrical and chemical properties compared to other group elements.

In sub-10 nm He ion beam milling (HIBM), it is necessary to solve the problem that the ion beam deviates from the irradiated position and affects not irradiated regions. Thus, it is suggested to fabricate sub-10 nm nanoholes on a thin membrane such as graphene [125-129]. As in Fig. 2(a), the graphene nanomesh is fixed in the air by Au anchor which is fabricated by EBL and silicon dioxide (SiO_2) etching. Since FIB milling of the nanomesh proceeds in the air, there is no He ion scattering by the atoms of the substrate under the irradiated surface. As another solution of the deviation, a simultaneous pulsed laser is used to increase photothermal energy of the He ion exposure region, which reduces ion implantation and defect [130]. On the other hand, when only a small part of a soft metal such as Au is milled, the Au milling can be finished before the He ions do a great deal of damage to the substrate. Therefore, plasmonic structures made of Au nanopatterns can be fabricated by HIBM [131].

He ion beam lithography (HIBL) is also useful for sub-10 nm fabrication [122, 132, 133], and it has several advantages compared to EBL. The beam size of the He ion beam is smaller than that of the SEM-based electron beam, so HIBL has a better resolution than EBL. Also, He ion beam has a smaller interaction volume and yields more secondary electrons than the electron beam for the same energy. This means that He ions have smaller proximity effects and higher exposure efficiency. In studies on sub-10 nm HIBL, there are cases where a resist becomes a final pattern [58] and a pattern transfer process such as etching or nanoimprint is performed with a resist pattern [134, 135]. In Fig. 2(b), a sub-10 nm width of Si grating was fabricated by HIBL. A resist pattern for the etch mask is fabricated with a He ion beam, and sub-10 nm gratings are fabricated by etching. When exposed to metal-organic resist ($Cr_8F_8(O_2CtBu)_{16}$), secondary or auger electrons generated on the resist surface undergo a chemical reaction with He

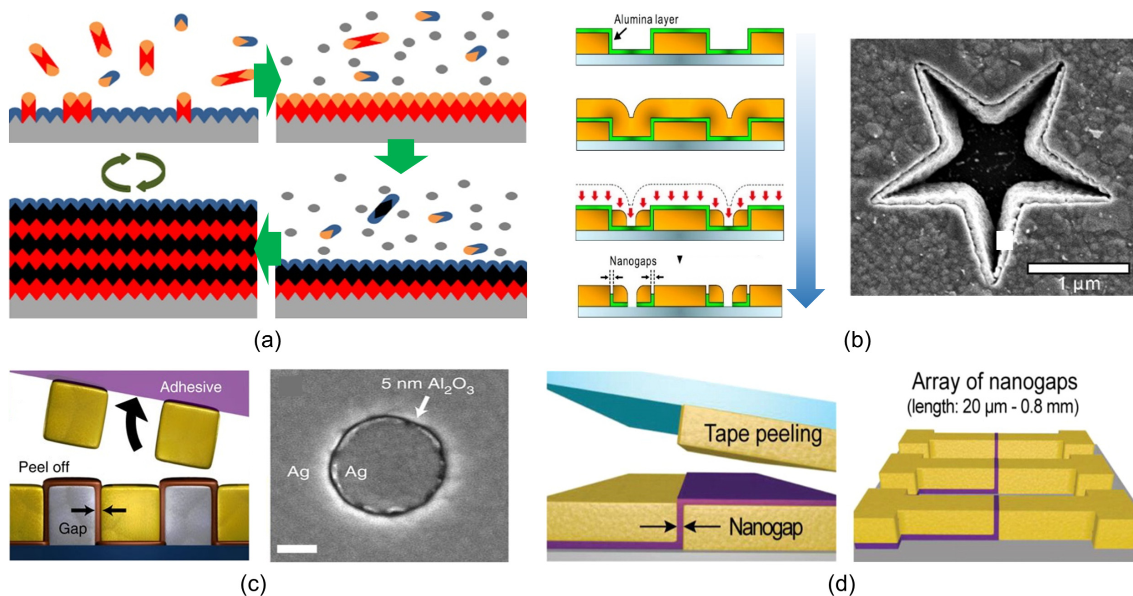

Fig. 3. Single-digit nanofabrication method using atomic layer deposition_1: (a) fabrication process of atomic layer deposition [138]; (b) fabrication process of atomic layer lithography and SEM image [140]; (c) schematic of atomic layer lithography using adhesive tape and SEM image [141]; (d) schematic of patterning of atomic layer lithography with adhesive tape using photolithography [91] (adapted with permission from Fig. 3 in Refs. [91, 138, 140, 141]).

ion, creating a chromium-oxide hard mask. This hard mask is suitable for dry etching used to etch Si and tungsten.

3.2 Neon ion beam

Ne ion beam lithography (NIBL) has been studied more than Ne ion beam milling (NIBM) in single-digit-dimension nanostructure fabrication. The He ion beam has high resolution fairly, but the sputter yield of less than 0.1 atom/incident ion is so low that it is not suitable for milling bulk semiconductors [122]. Thus, NIBM has been researched for sub-20 nm fabrication [136, 137], but studies on sub-10 nm are still insufficient due to the resolution decrease due to the substrate damage of Ne ions. Therefore, when fabricating sub-10 nm nanostructures using Ne ion beam, NIBL is used such as Fig. 2(c) [59]. The overall fabrication process is the same as that of HIBL but requires about ten times less exposure than He ion. On the other hand, since there is a problem of lowering the resolution due to substrate damage caused by the exposure beam that does not exist in EBL, it is necessary to avoid using He or Ne ion beams to produce large features.

3.3 Gallium ion beam

Ga ion beam milling (GIBM) can also fabricate sub-10 nm nanogap with proximity effect correction [60, 123] and breaking grain boundary [124]. Similar to the EBL, the proximity effect is caused by the irradiated ions affecting the periphery of the exposure target. Therefore, FIB milling for nanogap fabrication is carried out while predicting how much proximity effect will occur like EBL proximity effect correction. As in Fig. 2(d), a plasmonic 4 nm nanogap was fabricated using GIBM with proximity effect correction. Thus, by breaking the Au grain boundary using GIBM, a sub-2 nm nanogap can be created [124]. First, GIBM creates a nano junction containing a single grain boundary, and the second GIBM only exposes the junction to break the grain boundary. If Ga ion beam is used for sub-10 nm nanogap fabrication, the sputter yield rate is high and unintentional damage applied to the substrate can be quickly and stably fabricated than HIBM and NIBM. However, it is hard to fabricate sub-10 nm grating or nanodots due to the same disadvantage of EBL proximity effect correction.

4. Atomic layer deposition

Along with EBL and FIB techniques, ALD is regarded as one of the most important fabrication methods of a thin film for various materials [138, 139]. The single-digit fabrication technique with EBL and FIB has limitation in beam size and large-area fabrication. ALD can be used to overcome these limitations. Fig. 3(a) shows a typical ALD process [138]. The deposition occurs as a gaseous chemical precursor is pulsed and purged, resulting in the binary reaction of gas and surface. First, the reactant precursor A is pulsed in the chamber, resulting in conformal deposition of precursor A on the entire substrate surface. After unreacted precursor A is removed by purging chamber with an inert carrier gas, counter-reactant precursor B is pulsed, producing binary reaction with precursor A, resulting in single layer of the material. After removing unreacted precursor B, one cycle to fabricate one single layer is completed. By repeating this cycle n times, a thin film built from atomic layers can be fabricated.

ALD has two unique advantages compared to other deposition methods. First, precise thickness control at the monolayer

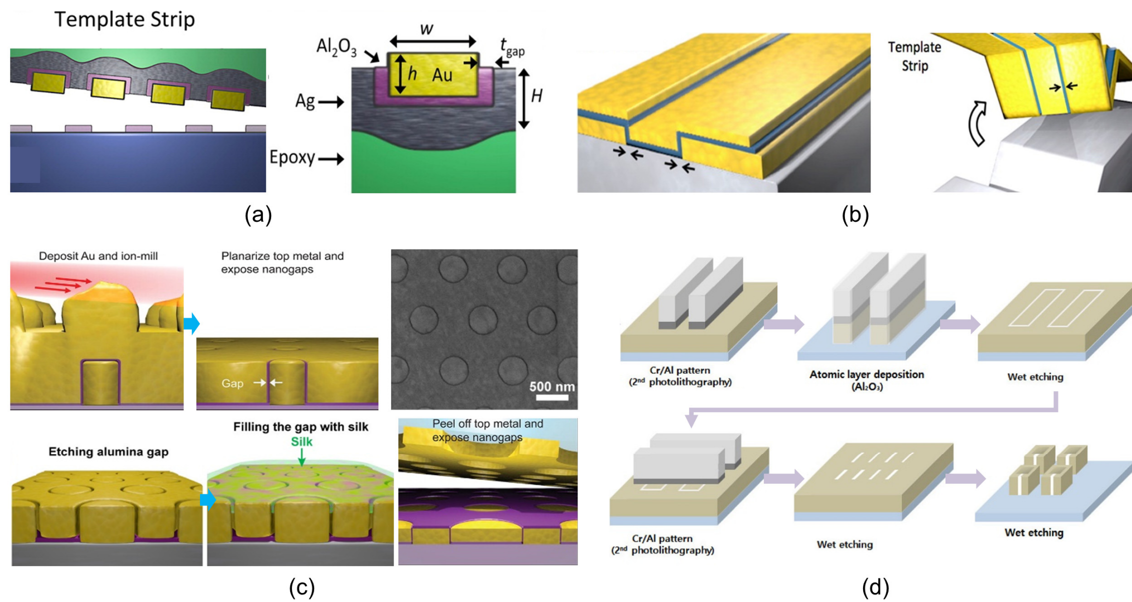

Fig. 4. Single-digit nanofabrication method using atomic layer deposition_2: (a) schematic of atomic layer lithography with template strip [84]; (b) schematic of split-wedge antennas fabrication using atomic layer lithography with template strip [142]; (c) schematic of atomic layer lithograph using glancing-angle ion beam polishing [143]; (d) fabrication process of a square-ring array with unsymmetrical single-digit gap using glanced ion beam [144] (adapted with permission from Fig. 4 in Refs. [84, 142, 143, 144]).

level (Å scale) is possible [139]. So, it has a slow deposition rate. The other advantage is the self-limiting property in that it does not build up more than a single layer. Thus, ALD films have higher conformality over the whole surface [139]. Therefore, the material is also deposited on the vertical wall, and a single-digit nanometer gap can be fabricated. In this chapter, we review the fabrication method for producing single-digit nanometer structures.

4.1 Atomic layer lithography

Atomic layer lithography (ALL) has been developed to fabricate single-digit nanometer structures using ALD [19, 84, 86, 90, 91, 140-144]. Fabrication methods for producing nanometer-scale gaps or cavities have been demonstrated using thin film deposition [145, 146]. However, these methods only achieve the fabrication of planar structures. In 2010, nanogaps of a vertical metal-insulator-metal (MIM) structure using ALD were demonstrated [140]. The left panel of Fig. 3(b) shows the fabrication process. First, arrays of Ag nanostructures arrays are fabricated using photolithography, and alumina (Al_2O_3) is deposited using ALD. After a second Ag layer is deposited, anisotropic ion beam milling is performed until the Al_2O_3 layer is revealed. Finally, the horizontal part of the Al_2O_3 layer is peeled off using a buffered oxide etchant, creating a single-digit nanogap. The right panel of Fig. 3(b) shows an SEM image of a fabricated nanogap structure. Since ALD can control the thickness in Å unit, single-digit nanogaps can be demonstrated. However, this method is limited to the fabrication of hollow structures. This fabrication method, combining ALD and plug-and-peel metal patterning for single-digit nanogaps, has been termed ALL.

Adhesive tape can be used to peel off the metal for planarization in ALL [90, 91, 141]. In 2013, nanostructures with down to 9.9 Å gap width were demonstrated without hollow structure by adhesive-tape ALL [141]. Single-digit nanogap is fabricated by depositing Alumina using ALD and metal using evaporator (the ‘plug’ process) in the patterned substrate is deposited, as shown in the left panel of Fig. 3(c). Adhesive tape can be used to peel off the metal film located above the substrate. The right panel of Fig. 3(c) shows an SEM image of the fabricated 5 nm gap structure. In 2016, micrometer-scale positive structures with single-digit scale nanogap were demonstrated by combining ALL and photolithography (Fig. 3(d)) [91]. After fabrication of a nanogap using ALL with adhesive tape, arrays of micrometer-scale structures are patterned by photolithography. This fabrication method shows the possibility to fabricate an array of patterns with a single-digit nanogap.

Similar to adhesive tape, epoxy can be used to peel off the metal in ALL [84, 142]. In 2015, a single-digit nanogap was demonstrated that is fabricated by patterning the template with stripes of epoxy [84]. Nanogaps are fabricated by depositing Al_2O_3 on patterned Au film using ALD. After evaporation of silver (Ag) (second layer of metal) on top of the Al_2O_3, nanogap structures are template-stripped and exposed (Fig. 4(a)). In 2016, split-wedge antennas with gap width down to 1 nm has been demonstrated using template stripping and ALL (Fig. 4(b)) [142].

Glancing-angle ion beam polishing also can be used to peel off metal in ALD [19, 86, 143]. Glancing-angle ion polishing is a milling technique using argon (Ar) ion. In 2016, 2 nm gap coaxial apertures have been demonstrated using glancing-angle ion

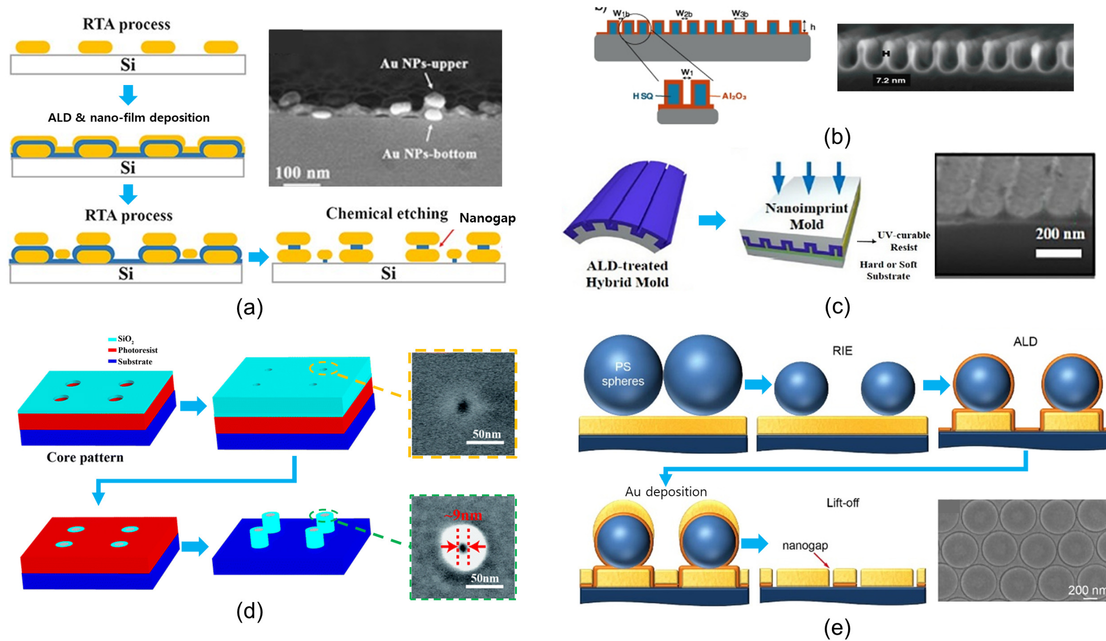

Fig. 5. Single-digit nanofabrication method combining ALD technique with other nanopatterning methods: (a) fabrication process of two NPs and single-digit nanogap using rapid thermal annealing [147]; (b) schematic of fabricating 5~9 nm gap with atomic layer deposition and nanoimprint lithography [149]; (c) schematic of fabricating single-digit nanogap by combining atomic layer deposition and nanoimprint lithography in the flexible substrate [150]; (d) fabrication process of nanoholes with the feature size 9 nm by improving the resolution of plasmonic lithography with atomic layer deposition [151]; (e) fabrication process of high dense arrays of annular nanogaps with sub-1 nm gap width by combining colloidal lithograph and atomic layer lithography [83] (adapted with permission from Fig. 5 in Refs. [83, 147, 149, 150, 151]).

beam polishing [143]. Fig. 4(c) shows the process of top metal planarization using a glancing-angle ion beam. After planarization, a single-digit nanogap of Al_2O_3 is revealed and can be controlled by ALD thickness. In 2018, nanogap structures filled with silk were demonstrated [86]. To fill nanogap with silk, Al_2O_3 of nanogap is etched and empty nanogap is filled with silk. This method shows the possibility to change the material of the nanogap, overcoming limited materials of ALD. This Al_2O_3 nanogap structure could be applied to an optical application such as optical trapping [19]. It is also possible to fabricate nanoaperture with single-digit nanogap using adhesive tape [90]. However, this method has a limitation in that size of the hole gap should be large enough to deposit metal (tens of micrometers to a few centimeters). On the other hand, in ALL using ion beam polishing, a second layer metal is deposited except for the positive nanohole aperture, making fabrication of a sub-micrometer scale hole gap possible.

Wet etching also can be used for planarization in ALL. In 2017, a split-ring resonator (SRR) with an unsymmetrical sub-10 nm gap was demonstrated using ALL, Ar ion beam milling, and photolithography [144]. The structure consists of a square-ring array with an unsymmetrical sub-10 nm gap. Fig. 4(d) shows the fabrication process of the SRRs. The first step is to make a chromium (Cr)/aluminum (Al) pattern on Cr/Au thin film by photolithography. Then, first ion milling eliminates part of the Cr/Au thin film, and Al_2O_3 is deposited by ALD, which determines the gap width of the final structure. Cr/Au thin films are deposited once again, and the ion milling mask is removed by wet etching. To fabricate an unsymmetrical gap, the sample is rotated by 90° and the previous steps are repeated except for the ALD step.

4.2 ALD techniques compatible with other nanopatterning methods

The fabrication method of 2~20 nm Al_2O_3 nanogap between Au NPs has been demonstrated using rapid thermal annealing (RTA) and ALD [147]. Fig. 5(a) shows the fabrication process and SEM image of fabricated two NPs and nanogap. First, Au film is deposited on Si substrate. Then, RTA is performed for 30 s at 500 ℃. Thus, the Au films converge with each other to produce NPs. An Al_2O_3 thin film is deposited and the previous steps are repeated from more NPs. By performing chemical etching of Al_2O_3, nanogap between two NPs can be fabricated. This fabrication method has advantages of low cost and large-area fabrication since this method does not use lithography technology.

NIL is a high throughput fabrication method that fabricates nanopattern precisely with low cost and large area [148]. However, it is hard to fabricate a single-digit nanometer structure with NIL, since the resolution of a stamp is not good enough (resolution limited to 15 nm). Nanoimprint templates with sub-10nm nanopatterns are fabricated using ALD and succeed to replicate and transfer nanopatterns [149]. Fig. 5(b) shows the template fabrication scheme and SEM images of the fabricated stamp and transferred pattern. Nanogaps width *W* of 15 nm

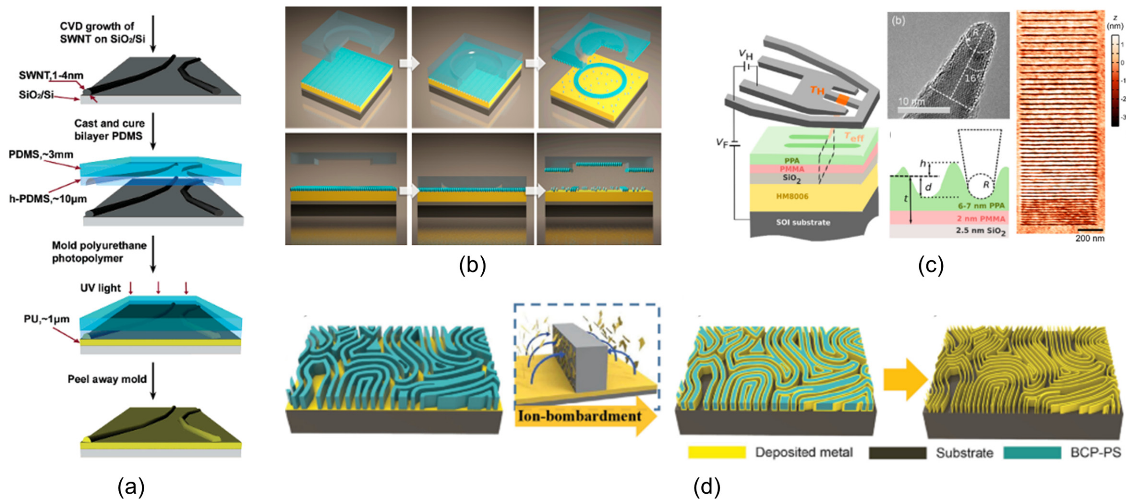

Fig. 6. Nanofabrication methods to achieve sub-10 nm nanostructures: (a) schematic of steps for polymer imprint lithography [154]; (b) schematic of self-collapse lithography (SCL) [160]; (c) schematic of thermal scanning probe lithography (t-SPL), SEM image of a sharp tip, and image of practical patterning line arrays [165]; (d) schematic of secondary sputtering lithography (SSL) enabling sidewall deposition with high resolution [167] (adapted with permission from Fig. 6 in Ref. [154, 160, 165, 167]).

are fabricated using EBL. Using ALD, the gap can be narrowed as thickness *d* of Al_2O_3 increases. After ALD of Al_2O_3, the final gap width is *W-2d*. In this paper, W is 17 nm and d is 4 or 6 nm. Therefore, NIL stamp with a gap width of 9 or 5 nm can be fabricated. Using this stamp, single-digit nanometer structure can be fabricated. In 2019, ALD was used to reduce the gap width of curved nanoimprint templates with flexible substrate [150]. In addition, PDMS are used to reduce the surface energy, so that stamp can easily release the polymer resist pattern. Single-digit nanometer structure on curved substrate can be imprinted by exposing UV light after stamping curved mold to soft substrate (Fig. 5(c)).

Nanoholes with feature sizes as small as 9 nm have been demonstrated by improving the resolution of plasmonic lithography with ALD [151]. Fig. 5(d) shows the fabrication process and SEM image of the inner gap after SiO_2 deposition. First, the core pattern can be fabricated by plasmonic lithography that uses Ag as a plasmonic cavity lens. Next, ALD is utilized to fabricate nano-core patterns by filling nanoholes with SiO_2, and the SiO_2 thickness should be equal to the width of the nano-core pattern. By etching SiO_2 and photoresist using reactive ion etching (RIE), the final structure of SiO_2 nanorings with sub-9 nm inner diameters can be generated. This fabrication method using plasmonic lithography has the advantage of low cost and high aspect ratios.

Highly dense arrays of annular nanogaps with sub-1 nm gap width over large areas have been demonstrated by combining colloidal lithography and ALD [83]. Fig. 5(e) shows the fabrication process and SEM image of fabricated narrow annular nanogap arrays. Polystyrene (PS) sphere monolayer covers metallic film on Si/SiO_2 substrate. Next, the PS sphere is shrunk by RIE and used as a mask for following ion beam etching. The ion beam etching is taken to remove the uncovered metal part. Then, deposition of Al_2O_3 is taken with ALD, and deposition thickness will determine gap width. After pilling metal with deposition of the metal film, a lift-off process is taken to remove the PS sphere and wet etch of the Al_2O_3 layer. Different from the ALL, this method combines ALD, lithography using PS, and lift off to fabricate single-digit-nanometer nanogaps array cost-effectively.

5. Unconventional nanofabrication methods for sub-10 nm resolution

Although nanopatterning processes mentioned above could achieve sub-10 nm resolution, these methods still have challenges, such as complex steps and costly systems, interrupting practical fabrication of nanostructures. To overcome these drawbacks, alternative nanofabrication methods have been researched in many fields. Thus, in this section, we describe emerging nanopatterning processes that can fabricate sub-10 nm nanostructures or single-digit scale nanogaps.

5.1 Fabrication of sub-10 nm nanostructures

NIL is a promising nanopatterning process for large-area fabrication of sub-10 nm nanopatterns because it follows the resolution of used molds [152, 153]. To fabricate the NIL mold with single-digit nanometer-scaled patterns with 1~4 nm width, single-walled carbon nanotubes (SWCNTs) are utilized [154]. Fig. 6(a) shows the steps for polymer imprint lithography. Using PDMS to transfer features of the geometry of the SWCNTs, the transparent mold is generated. Subsequently, contacting the mold with polyurethane (PU) and then curing it to UV light generate a precise replica of the nanostructure. Besides direct fabrication of molds with single-digit nanometer resolution, post-processing of fabricated molds has been studied actively to reduce the size of nanopatterns of the molds [155, 156]. An

NIL mold with 50 nm half-pitch lines is chemically etched by diluted hydrogen fluoride (HF) solution for shrinking linewidth of nanopatterns on the mold [157]. The linewidth of nanogratings is shrunk from 50 nm to 33, 20, and 9.3 nm after 132, 189, and 240 s of etching time of HF solution.

Collapse of nanopatterns has been mainly considered as an unwanted phenomenon, but rather an intentional collapse based on mathematical analysis such as calculating capillary force can make uniform nanostructures with high resolution [158]. Using capillary force-induced cohesion during the post-development and drying process, a new nanofabrication method to uniformly make collapsed nanopatterns has been demonstrated. As a follow-up study, the collapse of complex nanopatterns with a high aspect ratio has been also controlled [159] through engineering curvature, tilt, and asymmetric shape in the nanostructures. These processes have no proximity effect unlike photolithography and enable to control the single nanostructure. Furthermore, the self-collapse of polydimethylsiloxane (PDMS) has been used for the direct formation of small nanopatterns [160]. Fig. 6(b) is a schematic of self-collapse lithography (SCL). By controlling channel/reservoir geometry, adhesion, and bending stiffness of the PDMS, different collapse properties of the PDMS is achieved [161]. The PDMS stamp after the oxygen plasma process is conformally contacted with the self-assembled monolayer (SAM)-coated Au surface. After that the PDMS stamp is self-collapsed because of its load, selectively removing SAM layers.

Scanning probe lithography (SPL) has been regarded as another alternative nanopatterning process due to its extremely high resolution of used sharp tips [162, 163]. In particular, thermal SPL (t-SPL), relying on thermal decomposition of resists, has enabled to fabricate sub-20 nm nanostructures [164]. Si NWs are scribed at a half-pitch of 18.3 nm to a depth of 5 nm on a polyphthalaldehyde (PPA) layer with 9 nm thickness by t-SPL. Also, nanostructures with sub-10 nm feature size are fabricated on the Si substrate by using t-SPL [165]. Fig. 6(c) is a schematic of t-SPL, a SEM image of a sharp tip, and an image of practical patterning line arrays with half-pitches of 10, 14, 17, 21, and 30 nm at 600 °C and 24 nN. By optimizing conditions of t-SPL, 11 nm half-pitch nanopatterns are achieved on the surface of the PPA layer.

Sidewall deposition with a high spatial resolution also has been researched through secondary sputtering lithography (SSL), by which a target material is etched and adhered to the side surface of a pre-patterned template [166]. For example, Au nanopatterns with a high aspect ratio are fabricated on the single conventional block copolymer (BCP) template by SSL (Fig. 6(d)) [167]. SSL etches Au films on the substrate and simultaneously deposits them onto the sidewalls of the nanostructure template. As a result, these steps produce nanopatterns with small feature sizes (10 nm), a high aspect ratio (>5), and a high density (14000 line ea mm^{-1}). As a follow-up study, the ion bombardment process is applied to produce a high resolution nanogroove (HRN) structure with a narrow contact width (15 nm) [168]. After the platinum (Pt) is deposited on soft-imprinted nanopatterns, Ar plasma bombardment is conducted to deposit Pt particles onto the sidewall of the nanostructures, causing nanopatterns with an ultra-high aspect ratio (~20) and high resolution (15 nm).

5.2 Realization of single-digit-nanometer scale nanogaps

Not only nanostructures, but nanogaps with single-digit resolution have also been easily produced by NIL because of its excellent reverse transferring property [169]. In particular, sub-4 nm size nanogaps are straightforwardly fabricated by NIL and collapsing nanopatterns [170]. Fig. 7(a) is a procedure for the fabrication of nanofingers. After dielectric coating to the imprinted nanofingers with Au particles, the adjacent nanostructures are collapsed each other with a certain distance controlled by dielectric coating thickness, resulting in Au nanoparticles with nanogaps about 2~6 nm. As a follow-up study, plasmonic nanostructures are fabricated by NIL, deposition of an ultra-thin (2 nm) dielectric tetrahedral amorphous carbon (ta-C) film, and the collapse of nanofibers [171]. After nanowires are produced by NIL, the nanostructures coated with Ag and ta-C are collapsed. The fabricated nanogap size is precisely defined by the ta-C thickness, which leads to enhancement of electromagnetic (EM) field owing to gap-plasmon resonance.

Furthermore, collapsing nanopatterns could produce sharper nanogaps than existing nanofabrication methods, which the well-known example of is capillary-force-induced collapse lithography (CCL), as shown in Fig. 7(b) [172]. By modulating EBL conditions such as the electron beam dose (energy), development time, and structural characteristics of the column, the collapse of nanopillars can be controlled precisely. Also, CCL fabricates nanogap structures with various shapes such as flowers or bowties, enabling practical fabrication of nanogaps with sub-10 nm size plasmonic structures on demand. As a follow-up study, cascade domino lithography (CDL) is researched for the application of extreme photon squeezing [173]. Fig. 7(c) is a schematic of CDL and a SEM image of collapsed nanopatterns. Positive photoresists with different solubility in one developer are stacked on the substrate and patterned by EBL, followed by the cold development and the Au deposition. CDL goes beyond the fundamental limitation of EBL, the proximity effect, by collapsing nanopatterns intentionally.

While cracking has been generated accidentally during fabrication of nanostructures so considered as an undesirable phenomenon like collapsing, the controlled initiation of various channeled crack patterns enables to produce single-digit scale nanogaps uniformly and quickly [174-176]. For example, Au break junctions having sub-3 nm gaps are fabricated by a self-breaking based on the controlled crack formation (Fig. 7(d)) [75]. To fabricate uniform Au nanogaps, titanium nitride (TiN) and Au are coated on the Si substrate. Subsequently, TiN cantilevers as a nano-pulling stage are fabricated by selective etching of the Si. This causes cantilevers to be retracted in

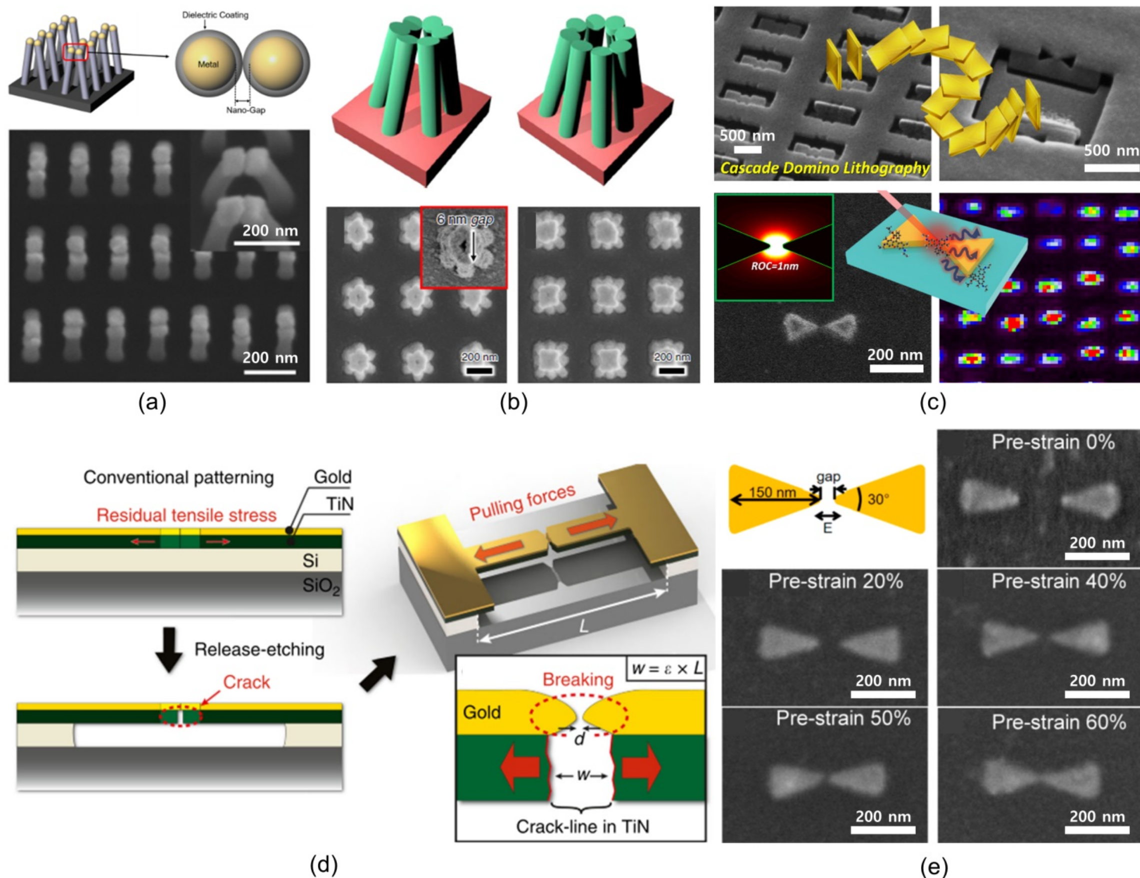

Fig. 7. Nanofabrication methods for achieving single-digit size nanogaps: (a) schematic and SEM images of collapsed nanofingers with single-digit resolution [170]; (b) schematic of flower-shaped nanogap structures and SEM images of flower structures with six and eight nanogaps. The structures are designed to form N nanogaps when the N columns fall over each other. The nanogap size is ~6 nm (inset of (b)) [172]; (c) schematic of cascade domino lithography (CDL), SEM images of fabricated nanogaps, and surface enhanced Raman spectroscopy (SERS) mapping results [173]; (d) schematic of fabricating sub-3 nm nanogaps using crack-defined Au break junction [75]; (e) schematic of specification of the bowtie structure and SEM images of nanostructures on the released PDMS substrate at different pre-strain [182] (adapted with permission from Fig. 7 in Refs. [75, 170, 172, 173, 182]).

opposite directions, breaking apart the Au film located on the TiN crack and generating Au nanogaps. Nanogaps are also fabricated on flexible substrates by swelling-controlled cracking [177]. Cr/Au electrodes are fabricated on a flexible polymer substrate by photolithography, sputtering, and lift-off processes. Subsequently, swelling of an organic solvent which is induced along a junction results in the generation of the nanogap on electrodes because the organic solvent permeates into the swelling layer under the electrodes.

Utilizing the difference of adhesion between substrates and materials has been another alternative nanofabrication method to produce sub-10 nm nanogaps [178]. Metal electrodes and devices with asymmetric sub-15 nm nanogaps are fabricated by adhesion lithography [179]. After the metal M1 with a metallophilic self-assembled monolayer (SAM) is selectively deposited on the substrate, metal M2 is deposited evenly over the M1 and the substrate. Subsequently, an adhesive tape selectively eliminates the M2 on the SAM by using the difference of adhesion between M2-substrate and M2-SAM, leaving M2-SAM-M1 arrays with sub-15 nm nanogaps. As a follow-up study, large-area and flexible electronics with nanogaps are realized by the adhesion lithography [39, 180]. In addition, nanotransfer printing based on adhesion difference between target substrates and functional materials has been also attractive because of its fine pattern resolution, simple process steps, and cost-effectiveness [181]. For the fabrication of sub-10 nm nanogaps, metal-assisted transfer printing is conducted on the PDMS substrate [182]. The elastic substrate is stretched with a pre-strain and then Au nanostructures are transferred from the Ag/Si substrate to the PDMS surface. By releasing pre-stretched PDMS to the original shape, the size of nanogaps is controlled easily. Fig. 7(e) is a specification of the bowtie structure and SEM images of Au nanostructures on the released PDMS substrate at pre-strain of 0 %, 20 %, 40 %, 50 %, and 60 %, showing successful fabrication of sub-10 nm Au nanogaps.

6. Applications

As sub-10 nm fabrication methods have been developed, the

 DOI 10.1007/s12206-021-0243-7

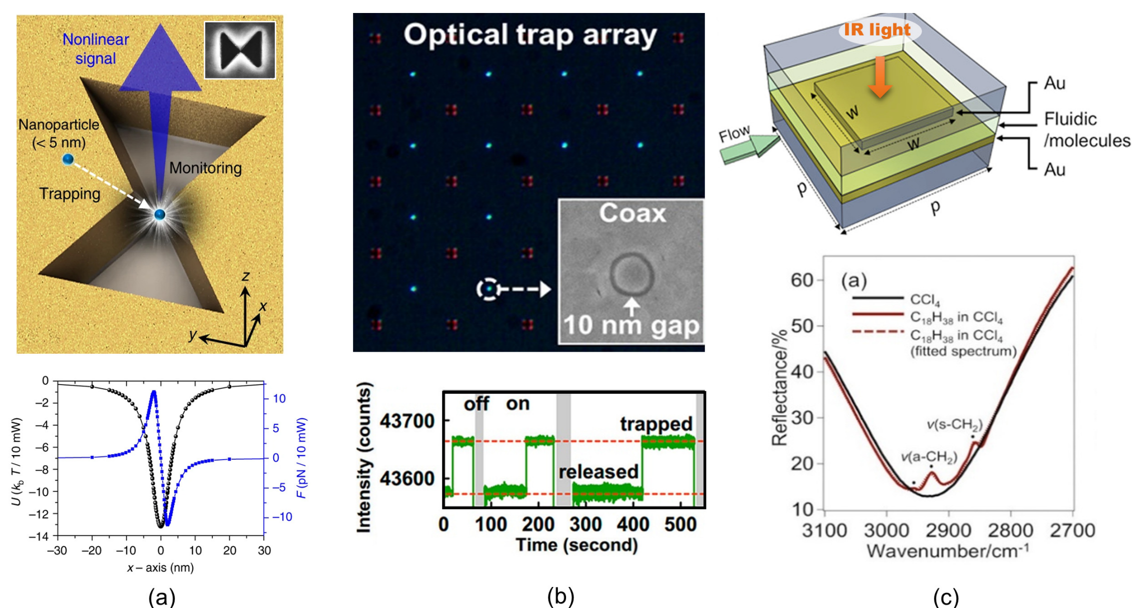

Fig. 8. Optical trapping and sensing devices: (a) schematic of tapered plasmonic nanoantenna which traps sub-5 nm NPs and generates a second-harmonic signal (upper). NP positions at the potential minimum point, middle of the x-axis (lower) [123]; (b) bright-field optical microscopy image of optical trapping array. Each coaxial aperture has a 10 nm gap (upper). Time trace of the transmitted intensity in trapping and releasing modes (lower) [19]; (c) schematic view of the single unit cell of the nanofluidic channel (upper). Strong coupling between target molecules and plasmonic gap induces distinct changes of reflectance spectra [85] (adapted with permission from Fig. 8 in Refs. [19, 85, 123]).

range of application becomes wider. The noteworthy phenomena which are excited between plasmonic gaps such as localization of electromagnetic field and surface plasmon resonance extend the measurable or observable range up to molecular or nanoparticle level when sensing [18, 20, 89, 90, 171] or imaging [80, 96, 183-187]. Moreover, light-matter interaction within the plasmonic nanostructures induces strong coupling, which enables the detection of quantum-level plasmonic response such as charge tunneling [74, 76, 93], Purcell effect [72, 80, 188], and Rabi splitting [78, 79, 179, 189, 190]. In this section, we classify applications depending on functionality.

6.1 Optical sensing and trapping devices

The strong interaction between subwavelength scale nanostructures and incident light amplifies output sensing signal and enhances trapping force. For this reason, optically stimulated plasmonic devices have been utilized for sensing and trapping devices for spectroscopy and real-time detection. For example, non-fluorescent detection with a tapered plasmonic antenna has been demonstrated for trapping NPs under 5 nm (Fig. 8(a)) [123]. Conventional fluorescent detection and single wavelength non-fluorescent detection require a phosphor attachment process for the trace tracking of target particles. However, this system does not need that process because the particles are trapped at the middle point of the bowtie antenna where the trapping force has the maximum value due to the field gradient. Because it exploits second harmonic illumination in plasmonic resonance within the cavity, it enables control of the trapping and the monitoring lights independently. Monitoring output signal and field strength gets stronger when the gap size decreases. 10 nm coaxial nanohole array has been also suggested as the trapping device (Fig. 8(b)) [19]. Because the electromagnetic field is highly localized at metallic aperture, which induces particles to be trapped between gaps, this array operates at low power and the target subject gets less damaged. Because the switching process between trapping and releasing is reversible, repetitive operating is possible. This system has a rapid speed of heat dissipation and high degree of freedom on design such as size and diameter of gap and thickness of the film. To improve detecting and sensing capabilities, it is important to increase the trapping spot area. Therefore, a fluidic system that widens the reaction area as the surface rather than point has been introduced [85]. It is composed of a sandwich structure of Au nanodisk and Au film and the Au nanodisks are arranged with distinct width and periodicity which determine tuning resonance frequency (Fig. 8(c)). The gap size is modulated from 10 nm to 100 nm, which is determined by the target number of quantifying molecules. The electric field and the magnetic field are localized between gaps under irradiation of x-polarized IR light. This field confinement leads to trapping the target molecules between plasmonic gaps, and strong resonance is generated when the target exists. This strong resonance induces the change of reflection spectrum depending on species and numbers of target molecules. For example, the reflection spectrum of octadecane ($C_{18}H_{38}/CCl_4$) differs from that of pure solvent (CCl_4) because different binding states by bonding and chemical composition induces specific strong coupling that expresses as distinct peaks in the spectrum.

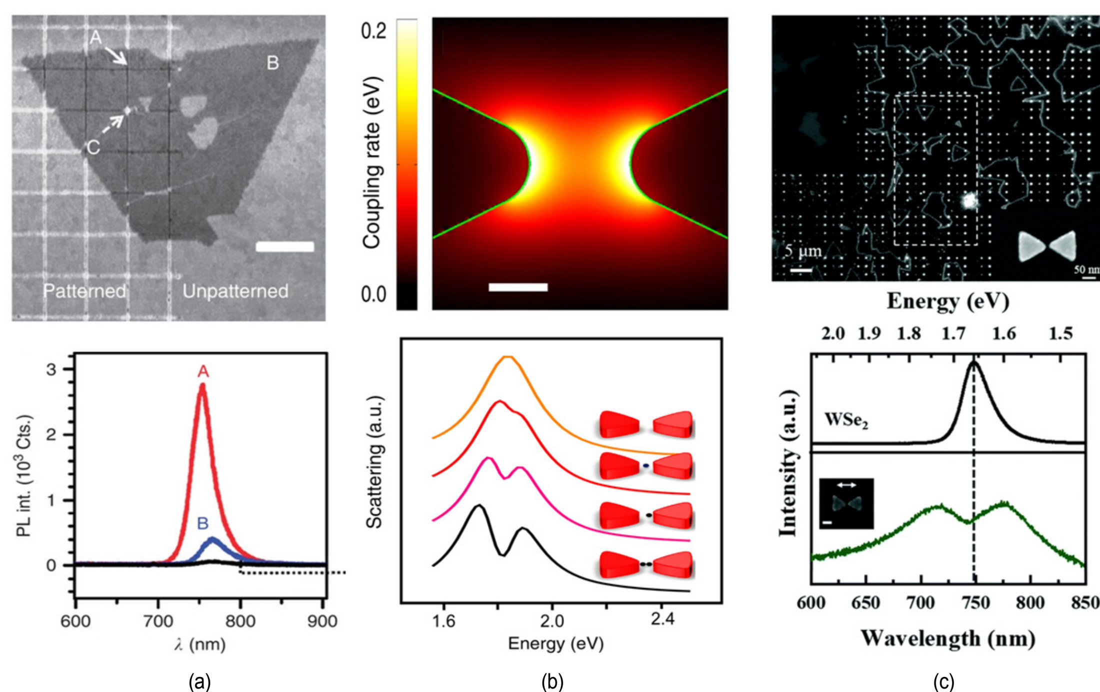

Fig. 9. Quantum plasmonic devices: (a) SEM image of TMDC monolayer flake on Au hybrid structure (upper). The PL intensity of TMDC at the intersection (position A) is much greater than that at the unpatterned region (position B) (lower) [73]; (b) distribution of the coupling rate of the bowtie plasmonic antenna. Strong coupling induces Rabi splitting of QD (upper). Whether Rabi splitting happens depends on the position and the quantity of QD (lower) [78]; (c) the dark-field optical micrograph of bowtie plasmonic antenna and monolayer TMDC. The inserted image on the top area is the bright field image of the white dashed zone. An SEM image of the Au bowtie is inserted on the bottom area (upper). Compared to the pure TMDC layer, TMDC on bow-tie antenna shows the split PL spectrum (lower) [193] (adapted with permission from Fig. 8 in Refs. [73, 78, 193]).

Quantum sensing devices which exploit quantum plasmonic effects get great attention recently because the unrevealing physics can be observed through these devices. Nanoscale plasmonic structures strongly interact with various kinds of emitters like quantum dot (QD) [81, 191, 192], transition metal dichalcogenide (TMDC) [72, 193], and upconversion nanoparticles [194-196], and show interesting phenomena such as gigantic photoluminescence enhancement and Rabi splitting. For example, a plasmonic system which consists of TMDC flakes and trenched Au substrate has been demonstrated to observe photoluminescent enhancement. (Fig. 9(a)) [73]. TMDC is integrated on the Au substrate which has patterned and unpatterned regions. Because the trench in a patterned area excites localized surface plasmon, which affects emission efficiency and excitation rate, the photoluminescence (PL) of TMDC on trench gets enhanced much more than that of TMDC in an unpatterned region. The PL intensity plot exhibits stark contrast between point A, which positions at the intersection of the trench, and point B on the unpatterned Au film. Rabi splitting phenomena due to light-matter interaction between the quantum emitter and single-digit nanostructure have been reported. For instance, Rabi splitting between the Ag antenna and QDs has been reported [78]. The plasmonic cavity confines the electric field and enables to shorten surface plasmon relaxation time and reduce mode volume (Fig. 9(b)). When the QDs locate inside the gaps because of interfacial capillary force, strong coupling between QDs and nanocavity is induced. The splitting of scattering peak, called Rabi splitting, is observed depending on the quantity and position of QDs. TMDC on the bow-tie antenna is another example of the optical systems exhibiting Rabi splitting (Fig. 9(c)) [193]. The monolayer TMDC, which is largely grown on the sapphire substrate, is transferred on the Au nanoantenna. The interaction between surface plasmon and exciton induces Rabi spitting, so the PL intensity gets split when the TMDC is integrated on the bowtie nanocavity. These quantum plasmonic devices have great potential to develop photo-detecting and photo-emitting systems with ultra-high quantum efficiency.

6.2 Plasmonic lenses for imaging and lithography

The nanopatterns of plasmonic lenses can be applied in imaging and lithography. These lenses confine incident light with ultra-small mode volume, and thus diffraction limit-free imaging and maskless lithography are possible. First, a multi-stage plasmonic lens (MPL) array and plasmonic flying head have been suggested for maskless lithography (Fig. 10(a)) [95]. The MPL arrays consist of a dumbbell-shaped aperture and coupler (inner ring) and reflector (outer ring). The input UV light excites propagating surface plasmons which propagate inward and are inverted as localized surface plasmons near the aperture.

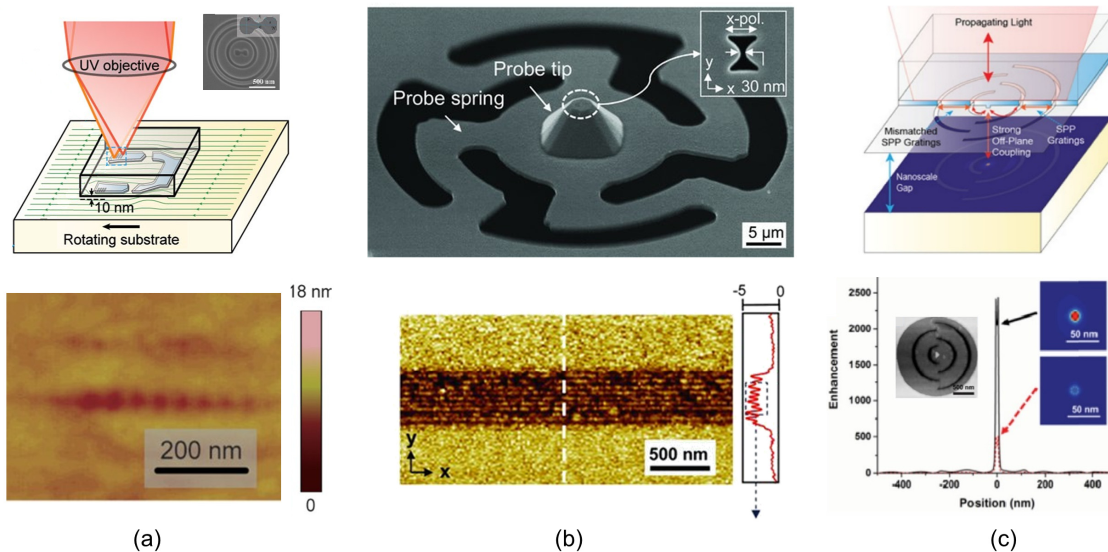

Fig. 10. Plasmonic lenses for imaging and lithography: (a) schematic of maskless lithography with multi-stage plasmonic lens (MPL) array and plasmonic flying head. The inserted SEM image shows MPL which contains ring couplers and a dumbbell-shaped aperture (upper). AFM image of patterned dots, which resolution is the 22-nm half-pitch (lower) [95]; (b) SEM image of circular contact probe. The inset image on the top-right corner shows the bow-tie shaped aperture at the probe tip (upper). AFM image of line array pattern which has 22-nm half-pitch resolution (lower) [197]; (c) schematic view of push-pin plasmonic lens (upper). The light gets enhanced at the center of the lens and the peak enhancement depends on the presence (black line) or absence (red line) of another Si wafer (lower) [96] (adapted with permission from Fig. 8 in Refs. [95, 96, 197]).

These localized surface plasmons help the incident beam to be confined within a deep sub-wavelength scale, which enables lithography with high spatial resolution. The output beam is confined to less than 50 nm and parallel patterns with a resolution of 22 nm half-pitch have been obtained. Secondly, 10 nm-gap-patterned plasmonic lithography, which overcomes the diffraction limit, has been suggested (Fig. 10(b)) [197]. Not only high speed but also high accuracy is obtained because it is a direct pattering system that contains a circular-type probe and bow-tie shaped aperture. The dense line array is patterned on the substrate and the full width at half maximum size is 22 nm. Lastly, a push-pin plasmonic lens achieving both high efficiency and high resolution in near-field imaging and lithography has been demonstrated (Fig. 10(c)) [96]. That lens consists of a set of the half-ring grating slit which induces a phase difference between the left-hand side and right-hand side propagating surface plasmon polaritons. The interference due to phase shift makes strong electric field enhancement along the off-plane direction. That plasmonic lens is utilized in high sensitivity photodetectors because the spot size is reduced by 1/20 times the wavelength of the incident beam.

6.3 Electronic devices

Metallic structures with a sub-10 nm gap can be used as electrodes and applied to nanoelectronic devices, such as electrical trapping device, a memory device, or a bio-molecular identifier. For example, the dielectrophoresis (DEP) technique has been suggested to trap NPs within a 9 nm gapped electrode (Fig. 11(a)) [91]. The trapping system is fabricated by ALL and the size of the Al_2O_3 gap is modulated by controlling deposition thickness. Because the minimum trapping voltage decreases as the width of nanogaps gets thinner, reducing the size of the gap helps to obtain high trapping efficiency. Trapping on/off modes are controlled by the operating frequency of the nanogap electrode and particles are trapped when the frequency is higher than a critical value. An electrical-optical dual-mode memory cell is another example of electronic devices; it contains waveguide-integrated plasmonic nanogaps with phase change material (Fig. 11(b)) [38]. Both electrical and optical pulse inverts the states of phase change material because the Au contacts are exploited as both electrodes and field-enhanced plasmonic gaps. The change in phase composition due to electrical write and erase pulses is quantified as both optical transmission and electrical resistance. Electrical resistance gets higher and optical transmission becomes lower in an amorphous state under erase pulse, and the opposite effect happens in the crystalline case. That memory cell has potential for optical-electrical switchable computing and communicating devices. As seen in Fig. 11(c), nanogaps which were tuned by piezo-actuating have been utilized for identification of nucleotide sequence by exploiting current tunneling [93]. The nucleotides are classified into four types including thymidine-, adenosine-, guanosine-, cytidine-5'-monophosphate and they have different molecular structures. Each time a unit nucleotide is passed, intensity peak I_p is obtained, which indicates affinity between the Au electrode and distinct nucleotide. If there are multiple kinds of nucleotides, the superposed I_p distribution is obtained. Therefore, by analyzing the histogram of the whole I_p data set, multiple nucleotides are identified

Table 1. Comparison chart for state-of-the-art top-down nanofabrication techniques.

	Minimum pattern resolution	Shapes	Advantages	Disadvantages	Refs.
Electron beam lithography (EBL)	~ 2 nm	Arbitrary	Very high resolution No need of masks High resolution	Proximity effect Slow speed High cost Need of resists	[117]
Focused ion beam (FIB)	~ 1.9 nm (Ne ion) ~ 0.5 nm (He ion) ~ 2 nm (Ga ion)	Arbitrary	No need of masks No need of resists Very high resolution	Ion contamination Slow speed Small patterning area	[59, 126, 127]
Atomic layer deposition (ALD)	< 1 nm	Ultra-thin film	High precision High resolution Good step coverage	High cost Slow speed	[141]
Nanoimprint lithography (NIL)	~ 1 nm	Arbitrary	Fast process Large-scale fabrication Cost-effective High resolution	Highly dependent on molds Hard to align Residual resist remains	[156]
Collapsing	~ 1 nm	Circle, triangle, rectangular	Compatible to any nanofabrication Controllable parameters High resolution	Limit of shape Not independent process	[175]
Scanning probe lithography (SPL)	< 10 nm	Arbitrary	Mechanical drawing Controllable depth High resolution	Slow speed Need of high temperature (if, thermal-SPL) Need of sharp tips	[167]
Cracking	~ 3 nm	Line	Simple mechanism Cost-effective Control cracks along crystal directions High resolution	Hard to control parameters Monotonous shape	[75]

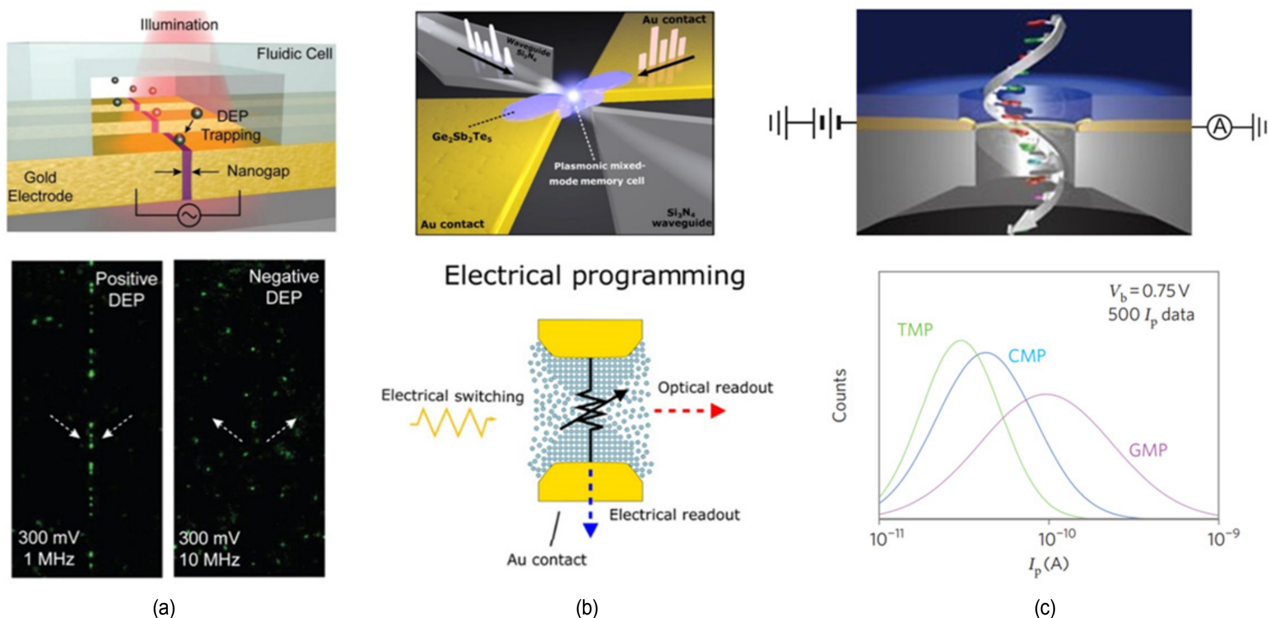

Fig. 11. Electronic devices: (a) schematic of DET trapping array. The nanogaps are exploited as electrodes and the electric field is localized at the gap (upper). Fluorescent image of the trapped mode in left and the dispersed mode in right (lower) [91]; (b) illustration of dually functional nanogap with a phase-change material (upper). Schematics of electrical programming in which electrical switching is read by both optical and electrical ways (lower) [38]; (c) conceptual illustration of DNA sequencing by scanning tunneling current (upper). Identifying nucleotides by analyzing statistical histogram (lower) [93] (adapted with permission from Fig. 8 in Refs. [38, 91, 93]).

by comparing single-base data. Aside from these, research for adapting single-digit nanostructure onto electronic devices continues to be actively studied such as ultra-small transistors [4], switches [198, 199], and sensors [23, 74, 200, 201].

7. Conclusions

In this review, we have presented the current state-of-the-art nanofabrication methods for achieving sub-10 nm nanostructures or nanogaps and then summarized features of the described processes, as seen Table 1. First, EBL and FIB can overcome the limit of resolution for fabricating sub-10 nm nanostructures. For example, AC-EBL and He or Ne FIB have been introduced as a means of reducing the beam size itself. Besides, errors in the development and pattern transfer processes have been reduced by using resists with high resolution and exposing smaller areas than the desired pattern size to prevent the proximity effect.

Second, promising technologies based on ALD have been introduced for the precise fabrication of single-digit nanostructures. ALD can be used to conformally deposit atomic-scale layers on arbitrary surfaces. In particular, ALL can be used to manufacture nanogaps on plain metal substrates by depositing materials on the sidewall of nanostructures and plugging and peeling materials. Furthermore, ALD has been integrated with other methods such as RTA, NIL, plasmonic lithography, and colloidal lithography for easily fabricating sub-10 nm size nanostructures.

Third, unconventional nanofabrication methods to obtain sub-10 nm nanostructures or single-digit size nanogaps have been discussed. In particular, NIL and collapsing can be applied to fabricate both nanostructures and nanogaps because they replicate nanostructures easily based on the mechanical process. SPL and sidewall deposition are also used to generate sub-10 nm nanopatterns. On the other hand, cracking and the difference in adhesion are mainly used to fabricate single-digit scale nanogaps.

Lastly, state-of-the-art applications of sub-10 nm size nanostructures involving optical trapping or sensing, imaging, and electronic devices have been studied. Optical devices can be utilized for precise devices such as spectroscopy, sensing, and optical trapping. Quantum plasmonic devices also can be a great achievement because they show interesting phenomena such as photoluminescent enhancement and Rabi splitting. Also, nanopatterned plasmonic lenses can be applied to limit-free imaging and maskless lithography. Moreover, metallic structures with sub-10 nm size nanogaps are utilized as electronic devices, such as electrical trapping devices, memory devices, or biological DNA identifiers.

Likewise, sub-10 nm nanostructures have been fabricated through various optical, mechanical, and chemical methods and are widely used in many applications. Despite these great achievements, ultra-precise nanofabrication methods are worthy to be developed in the direction of scalable fabrication [202] and high yield rate of single-digit scale nanostructures. By integrating established nanopatterning methods which are EBL, FIB, and ALD with unconventional methods such as NIL, collapsing, and cracking, large-area production of sub-10 nm nanostructures will be realized.

Acknowledgments

This work was financially supported by the National Research Foundation (NRF) grant (CAMM-2019M3A6B3030637) funded by the Ministry of Science and ICT (MSIT) of the Korean government. I.K. acknowledges the NRF Sejong Science fellowship (NRF-2021R1C1C2004291) funded by the MSIT of the Korean government. Y.K acknowledges a fellowship from the Hyundai Motor *Chung Mong-Koo* Foundation.

Nomenclature

AC-EBL : Aberration-corrected electron beam lithography
Ag : Silver
Al : Aluminum
Al_2O_3 : Aluminium oxide, Alumina
ALD : Atomic layer deposition
ALL : Atomic layer lithography
Ar : Argon
Au : Gold
BCP : Block copolymer
BSE : Backscattered electron
CCL : Capillary-force-induced collapse lithography
CDL : Cascade domino lithography
Cr : Chromium
DEP : Dielectrophoresis
EBL : Electron beam lithography
EM : Electromagnetic
FIB : Focused ion beam
Ga : Gallium
Ge : Germanium
GFIS : Gas field ion source
GIBM : Ga ion beam milling
He : Helium
HF : Hydrogen fluoride
HIBL : He ion beam lithography
HIBM : He ion beam milling
HRN : High resolution nanogroove
HSQ : Hydrogen silsesquioxane
LIL : Laser interference lithography
LMIS : Liquid metal ion source
MIM : Metal-insulator-metal
MPL : Multi-stage plasmonic lens
Ne : Neon
NIBL : Ne ion beam lithography
NIBM : Ne ion beam milling
NIL : Nanoimprint lithography
NPs : Nanoparticles
PDMS : Polydimethylsiloxane
PL : Photoluminescence

PPA : Polyphthalaldehyde
PS : Polystyrene
Pt : Platinum
PU : Polyurethane
QD : Quantum dot
RIE : Reactive ion etching
RTA : Rapid thermal annealing
SAM : Self-assembled monolayer
SCL : Self-collapse lithography
SE : Secondary electron
SEM : Scanning electron microscope
Si : Silicon
SiO_2 : Silicon dioxide
SPL : Scanning probe lithography
SRR : Split-ring resonator
SSL : Secondary sputtering lithography
STEM : Scanning transmission electron microscope
SWCNTs : Single-walled carbon nanotubes
ta-C : Tetrahedral amorphous carbon
TiN : Titanium nitride
TMDC : Transition metal dichalcogenide
t-SPL : Thermal scanning probe lithography

References

[1] S.-Y. Cho, H.-W. Yoo, J. Y. Kim, W.-B. Jung, M. L. Jin, J.-S. Kim, H.-J. Jeon and H.-T. Jung, High-resolution p-type metal oxide semiconductor nanowire array as an ultrasensitive sensor for volatile organic compounds, *Nano Letters*, 16 (7) (2016) 4508-4515.

[2] Y. Y. Choi, T. Teranishi and Y. Majima, Robust pt-based nanogap electrodes with 10 nm scale ultrafine linewidth, *Applied Physics Express*, 12 (2) (2019) 025002.

[3] A. Cui, H. Dong and W. Hu, Nanogap electrodes towards solid state single-molecule transistors, *Small*, 11 (46) (2015) 6115-6141.

[4] S. J. Lee, J. Kim, T. Tsuda, R. Takano, R. Shintani, K. Nozaki and Y. Majima, Single-molecule single-electron transistor (sm-set) based on π-conjugated quinoidal-fused oligosilole and heteroepitaxial spherical au/pt nanogap electrodes, *Applied Physics Express*, 12 (12) (2019) 125007.

[5] J. Park, D. Das, M. Ahn, S. Park, J. Hur and S. Jeon, Improved optical performance of multi-layer mos2 phototransistor with see-through metal electrode, *Nano Convergence*, 6 (1) (2019) 32.

[6] V. R. Murnal and C. Vijaya, A quasi-ballistic drain current, charge and capacitance model with positional carrier scattering dependency valid for symmetric dg mosfets in nanoscale regime, *Nano Convergence*, 6 (1) (2019) 19.

[7] R.-H. Horng, Y.-C. Lai and L.-H. Lai, Deep-ultraviolet leds fabricated by nanoimprinting, *ECS J. of Solid State Science and Technology*, 9 (1) (2019) 015005.

[8] I. Kim, M. A. Ansari, M. Q. Mehmood, W. S. Kim, J. Jang, M. Zubair, Y. K. Kim and J. Rho, Stimuli-responsive dynamic metaholographic displays with designer liquid crystal modulators, *Advanced Materials*, 32 (50) (2020) 2004664.

[9] G.-Y. Lee, G. Yoon, S.-Y. Lee, H. Yun, J. Cho, K. Lee, H. Kim, J. Rho and B. Lee, Complete amplitude and phase control of light using broadband holographic metasurfaces, *Nanoscale*, 10 (9) (2018) 4237-4245.

[10] G. Yoon, D. Lee, K. T. Nam and J. Rho, Pragmatic metasurface hologram at visible wavelength: the balance between diffraction efficiency and fabrication compatibility, *ACS Photonics*, 5 (5) (2017) 1643-1647.

[11] I. Kim, G. Yoon, J. Jang, P. Genevet, K. T. Nam and J. Rho, Outfitting next generation displays with optical metasurfaces, *ACS Photonics*, 5 (10) (2018) 3876-3895.

[12] Y.-J. Jung, S.-Y. Cho, J.-W. Jung, S.-Y. Kim and J.-H. Lee, Influence of indium-tin-oxide and emitting-layer thicknesses on light outcoupling of perovskite light-emitting diodes, *Nano Convergence*, 6 (1) (2019) 26.

[13] M. A. Ansari, I. Kim, I. D. Rukhlenko, M. Zubair, S. Yerci, T. Tauqeer, M. Q. Mehmood and J. Rho, Engineering spin and antiferromagnetic resonances to realize an efficient direction-multiplexed visible meta-hologram, *Nanoscale Horizons*, 5 (1) (2020) 57-64.

[14] G. Yoon, J. Kim, J. Mun, D. Lee, K. T. Nam and J. Rho, Wavelength-decoupled geometric metasurfaces by arbitrary dispersion control, *Communications Physics*, 2 (1) (2019) 129.

[15] M. A. Ansari, I. Kim, D. Lee, M. H. Waseem, M. Zubair, N. Mahmood, T. Badloe, S. Yerci, T. Tauqeer, M. Q. Mehmood and J. Rho, A spin-encoded all-dielectric metahologram for visible light, *Laser & Photonics Reviews*, 13 (5) (2019) 1900065.

[16] G. Yoon, D. Lee, K. T. Nam and J. Rho, "Crypto-display" in dual-mode metasurfaces by simultaneous control of phase and spectral responses, *ACS Nano*, 12 (7) (2018) 6421-6428.

[17] Z. Li, I. Kim, L. Zhang, M. Q. Mehmood, M. S. Anwar, M. Saleem, D. Lee, K. T. Nam, S. Zhang, B. Luk'yanchuk, Y. Wang, G. Zheng, J. Rho and C.-W. Qiu, Dielectric meta-holograms enabled with dual magnetic resonances in visible light, *ACS Nano*, 11 (9) (2017) 9382-9389.

[18] D. X. Ji, A. Cheney, N. Zhang, H. M. Song, J. Gao, X. Zeng, H. F. Hu, S. H. Jiang, Z. F. Yu and Q. Q. Gan, Efficient mid-infrared light confinement within sub-5-nm gaps for extreme field enhancement, *Advanced Optical Materials*, 5 (17) (2017) 1700223.

[19] D. Yoo, K. L. Gurunatha, H. K. Choi, D. A. Mohr, C. T. Ertsgaard, R. Gordon and S. H. Oh, Low-power optical trapping of nanoparticles and proteins with resonant coaxial nanoaperture using 10 nm gap, *Nano Letters*, 18 (6) (2018) 3637-3642.

[20] W. Zhang, L. Huang, C. Santschi and O. J. F. Martin, Trapping and sensing 10 nm metal nanoparticles using plasmonic dipole antennas, *Nano Letters*, 10 (3) (2010) 1006-1011.

[21] D. Lee, Y. Yang, G. Yoon, M. Kim and J. Rho, Resolution enhancement of fluorescence microscopy using encoded patterns from all-dielectric metasurfaces, *Applied Physics Letters*, 115 (10) (2019) 101102.

[22] M. Kim, K. Yao, G. Yoon, I. Kim, Y. Liu and J. Rho, A broadband optical diode for linearly polarized light using symmetry-

breaking metamaterials, *Advanced Optical Materials*, 5 (19) (2017) 1700600.

[23] Y. Ma, B. Dong and C. Lee, Progress of infrared guided-wave nanophotonic sensors and devices, *Nano Convergence*, 7 (1) (2020) 12.

[24] A. Minovich, J. Farnell, D. N. Neshev, I. McKerracher, F. Karouta, J. Tian, D. A. Powell, I. V. Shadrivov, H. H. Tan, C. Jagadish and Y. S. Kivshar, Liquid crystal based nonlinear fishnet metamaterials, *Applied Physics Letters*, 100 (12) (2012) 121113.

[25] A. Minovich, D. N. Neshev, D. A. Powell, I. V. Shadrivov and Y. S. Kivshar, Tunable fishnet metamaterials infiltrated by liquid crystals, *Applied Physics Letters*, 96 (19) (2010) 193103.

[26] T. Badloe, I. Kim and J. Rho, Biomimetic ultra-broadband perfect absorbers optimised with reinforcement learning, *Physical Chemistry Chemical Physics*, 22 (4) (2020) 2337-2342.

[27] T. Badloe, I. Kim and J. Rho, Moth-eye shaped on-demand broadband and switchable perfect absorbers based on vanadium dioxide, *Scientific Reports*, 10 (1) (2020) 4522.

[28] T. Badloe, J. Mun and J. Rho, Metasurfaces-based absorption and reflection control: Perfect absorbers and reflectors, *J. of Nanomaterials*, 2017 (1) (2017) 2361042.

[29] I. Kim, S. So, A. S. Rana, M. Q. Mehmood and J. Rho, Thermally robust ring-shaped chromium perfect absorber of visible light, *Nanophotonics*, 7 (11) (2018) 1827-1833.

[30] D. Lee, S. Y. Han, Y. Jeong, D. M. Nguyen, G. Yoon, J. Mun, J. Chae, J. H. Lee, J. G. Ok and G. Y. Jung, Polarization-sensitive tunable absorber in visible and near-infrared regimes, *Scientific Reports*, 8 (1) (2018) 12393.

[31] D. M. Nguyen, D. Lee and J. Rho, Control of light absorbance using plasmonic grating based perfect absorber at visible and near-infrared wavelengths, *Scientific Reports*, 7 (1) (2017) 2611.

[32] G. Yoon, S. So, M. Kim, J. Mun, R. Ma and J. Rho, Electrically tunable metasurface perfect absorber for infrared frequencies, *Nano Convergence*, 4 (1) (2017) 36.

[33] J. Jang, T. Badloe, Y. Yang, T. Lee, J. Mun and J. Rho, Spectral modulation through the hybridization of mie-scatterers and quasi-guided mode resonances: realizing full and gradients of structural color, *ACS Nano*, 14 (11) (2020) 15317-15326.

[34] I. Kim, J. Yun, T. Badloe, H. Park, T. Seo, Y. Yang, J. Kim, Y. Chung and J. Rho, Structural color switching with a doped indium-gallium-zinc-oxide semiconductor, *Photonics Research*, 8 (9) (2020) 1409-1415.

[35] M. Kim, I. Kim, J. Jang, D. Lee, K. T. Nam and J. Rho, Active color control in a metasurface by polarization rotation, *Applied Sciences*, 8 (6) (2018) 982.

[36] T. Lee, J. Jang, H. Jeong and J. Rho, Plasmonic-and dielectric-based structural coloring: from fundamentals to practical applications, *Nano Convergence*, 5 (1) (2018) 1.

[37] J. Jang, T. Badloe, Y. C. Sim, Y. Yang, J. Mun, T. Lee, Y.-H. Cho and J. Rho, Full and gradient structural colouration by lattice amplified gallium nitride mie-resonators, *Nanoscale*, 12 (41) (2020) 21392-21400.

[38] N. Farmakidis, N. Youngblood, X. Li, J. Tan, J. L. Swett, Z. Cheng, C. D. Wright, W. H. Pernice and H. Bhaskaran, Plasmonic nanogap enhanced phase-change devices with dual electrical-optical functionality, *Science Advances*, 5 (11) (2019) eaaw2687.

[39] D. G. Georgiadou, Y. H. Lin, J. Lim, S. Ratnasingham, M. A. McLachlan, H. J. Snaith and T. D. Anthopoulos, High responsivity and response speed single-layer mixed-cation lead mixed-halide perovskite photodetectors based on nanogap electrodes manufactured on large-area rigid and flexible substrates, *Advanced Functional Materials*, 29 (28) (2019) 1901371.

[40] H. Kang, S. Y. Cho, J. Ryu, J. Choi, H. Ahn, H. Joo and H. T. Jung, Multiarray nanopattern electronic nose (e-nose) by high-resolution top-down nanolithography, *Advanced Functional Materials*, 30 (27) (2020) 2002486.

[41] M. Kim, Y. Kim and J. Rho, Spin-valley locked topological edge states in a staggered chiral photonic crystal, *New J. of Physics*, 22 (11) (2020) 113022.

[42] M. Kim, D. Lee, T. H. Kim, Y. Yang, H. J. Park and J. Rho, Observation of enhanced optical spin hall effect in a vertical hyperbolic metamaterial, *ACS Photonics*, 6 (10) (2019) 2530-2536.

[43] M. Kim, D. Lee, B. Ko and J. Rho, Diffraction-induced enhancement of optical spin hall effect in a dielectric grating, *APL Photonics*, 5 (6) (2020) 066106.

[44] K. Yoo, W. Lee, K. Kang, I. Kim, D. Kang, D. K. Oh, M. C. Kim, H. Choi, K. Kim, M. Kim, J. D. Kim, I. Park and J. G. Ok, Low-temperature large-area fabrication of zno nanowires on flexible plastic substrates by solution-processible metal-seeded hydrothermal growth, *Nano Convergence*, 7 (1) (2020) 24.

[45] A. S. Rana, I. Kim, M. A. Ansari, M. S. Anwar, M. Saleem, T. Tauqeer, A. Danner, M. Zubair, M. Q. Mehmood and J. Rho, Planar achiral metasurfaces-induced anomalous chiroptical effect of optical spin isolation, *ACS Applied Materials & Interfaces*, 12 (43) (2020) 48899-48909.

[46] S.-J. Kim, I. Kim, S. Choi, H. Yoon, C. Kim, Y. Lee, C. Choi, J. Son, Y. W. Lee, J. Rho and B. Lee, Reconfigurable all-dielectric fano metasurfaces for strong full-space intensity modulation of visible light, *Nanoscale Horizons*, 5 (7) (2020) 1088-1095.

[47] I. C. Khoo, D. H. Werner, X. Liang, A. Diaz and B. Weiner, Nanosphere dispersed liquid crystals for tunable negative-zero-positive index of refraction in the optical and terahertz regimes, *Optics Letters*, 31 (17) (2006) 2592-2594.

[48] Y. Chen, B. Ai and Z. J. Wong, Soft optical metamaterials, *Nano Convergence*, 7 (1) (2020) 18.

[49] P. N. Navya, A. Kaphle, S. P. Srinivas, S. K. Bhargava, V. M. Rotello and H. K. Daima, Current trends and challenges in cancer management and therapy using designer nanomaterials, *Nano Convergence*, 6 (1) (2019) 23.

[50] J.-H. Lee, E.-J. Chae, S.-J. Park and J.-W. Choi, Label-free detection of γ-aminobutyric acid based on silicon nanowire biosensor, *Nano Convergence*, 6 (1) (2019) 13.

[51] N. Yu and F. Capasso, Flat optics with designer metasurfaces,

Nature Materials, 13 (2) (2014) 139-150.

[52] X. Yin, Z. Ye, J. Rho, Y. Wang and X. Zhang, Photonic spin hall effect at metasurfaces, *Science*, 339 (6126) (2013) 1405-1407.

[53] H. Ren, X. Fang, J. Jang, J. Burger, J. Rho and S. A. Maier, Complex-amplitude metasurface-based orbital angular momentum holography in momentum space, *Nature Nanotechnology*, 15 (11) (2020) 948-955.

[54] Y. H. Wang, I. Kim, R. C. Jin, H. Jeong, J. Q. Li, Z. G. Dong and J. Rho, Experimental verification of asymmetric transmission in continuous omega-shaped metamaterials, *RSC Advances*, 8 (67) (2018) 38556-38561.

[55] J. Jang, H. Jeong, G. W. Hu, C. W. Qiu, K. T. Nam and J. Rho, Kerker-conditioned dynamic cryptographic nanoprints, *Advanced Optical Materials*, 7 (4) (2019) 1801070-1801070.

[56] C.-W. Lee, H. J. Choi and H. Jeong, Tunable metasurfaces for visible and swir applications, *Nano Convergence*, 7 (1) (2020) 3.

[57] F. I. Allen, N. R. Velez, R. C. Thayer, N. H. Patel, M. A. Jones, G. F. Meyers and A. M. Minor, Gallium, neon and helium focused ion beam milling of thin films demonstrated for polymeric materials: study of implantation artifacts, *Nanoscale*, 11 (3) (2019) 1403-1409.

[58] R. Kumar, M. Chauhan, M. G. Moinuddin, S. K. Sharma and K. E. Gonsalves, Development of nickel-based negative tone metal oxide cluster resists for sub-10 nm electron beam and helium ion beam lithography, *ACS Applied Materials & Interfaces*, 12 (17) (2020) 19616-19624.

[59] D. Winston, V. R. Manfrinato, S. M. Nicaise, L. L. Cheong, H. Duan, D. Ferranti, J. Marshman, S. McVey, L. Stern, J. Notte, and K. K. Berggren, Neon ion beam lithography (nibl), *Nano Letters*, 11 (10) (2011) 4343-4347.

[60] M.-K. Kim, H. Sim, S. J. Yoon, S.-H. Gong, C. W. Ahn, Y.-H. Cho and Y.-H. Lee, Squeezing photons into a point-like space, *Nano Letters*, 15 (6) (2015) 4102-4107.

[61] E. Højlund-Nielsen, J. Clausen, T. Mäkela, L. H. Thamdrup, M. Zalkovskij, T. Nielsen, N. Li Pira, J. Ahopelto, N. A. Mortensen and A. Kristensen, Plasmonic colors: toward mass production of metasurfaces, *Advanced Materials Technologies*, 1 (7) (2016) 1600054.

[62] S. Murthy, H. Pranov, N. A. Feidenhans'l, J. S. Madsen, P. E. Hansen, H. C. Pedersen and R. Taboryski, Plasmonic color metasurfaces fabricated by a high speed roll-to-roll method, *Nanoscale*, 9 (37) (2017) 14280-14287.

[63] J. S. Wi, S. Lee, S. H. Lee, D. K. Oh, K. T. Lee, I. Park, M. K. Kwak and J. G. Ok, Facile three-dimensional nanoarchitecturing of double-bent gold strips on roll-to-roll nanoimprinted transparent nanogratings for flexible and scalable plasmonic sensors, *Nanoscale*, 9 (4) (2017) 1398-1402.

[64] G. Yoon, K. Kim, D. Huh, H. Lee and J. Rho, Single-step manufacturing of hierarchical dielectric metalens in the visible, *Nature Communications*, 11 (1) (2020) 2268.

[65] K. Kim, G. Yoon, S. Baek, J. Rho and H. Lee, Facile nanocasting of dielectric metasurfaces with sub-100 nm resolution, *ACS Applied Materials & Interfaces*, 11 (29) (2019) 26109-26115.

[66] P. Jacquet, B. Bouteille, R. Dezert, J. Lautru, R. Podor, A. Baron, J. Teisseir, J. Jupille, R. Lazzari and I. Gozhyk, Periodic arrays of diamond-shaped silver nanoparticles: From scalable fabrication by template-assisted solid-state dewetting to tunable optical properties, *Advanced Functional Materials*, 29 (28) (2019) 1901119.

[67] T. Das Gupta, L. Martin-Monier, W. Yan, A. Le Bris, T. Nguyen-Dang, A. G. Page, K. T. Ho, F. Yesilkoy, H. Altug, Y. Qu and F. Sorin, Self-assembly of nanostructured glass metasurfaces via templated fluid instabilities, *Nature Nanotechnology*, 14 (4) (2019) 320-327.

[68] C. Matricardi, J. L. Garcia-Pomar, P. Molet, L. A. Perez, M. I. Alonso, M. Campoy-Quiles and A. Mihi, High-throughput nanofabrication of metasurfaces with polarization-dependent response, *Advanced Optical Materials*, 8 (20) (2020) 2000786.

[69] S. Wu, Y. Ye, H. Duan, Y. Gu and L. Chen, Large-area, optical variable-color metasurfaces based on pixelated plasmonic nanogratings, *Advanced Optical Materials*, 7 (7) (2019) 1801302.

[70] V. B. Nam, T. T. Giang, S. Koo, J. Rho and D. Lee, Laser digital patterning of conductive electrodes using metal oxide nanomaterials, *Nano Convergence*, 7 (1) (2020) 23.

[71] T. Lee, C. Lee, D. K. Oh, T. Badloe, J. G. Ok and J. Rho, Scalable and high-throughput top-down manufacturing of optical metasurfaces, *Sensors*, 20 (15) (2020) 4108.

[72] K.-D. Park, T. Jiang, G. Clark, X. Xu and M. B. Raschke, Radiative control of dark excitons at room temperature by nano-optical antenna-tip purcell effect, *Nature Nanotechnology*, 13 (1) (2018) 59-64.

[73] Z. Wang, Z. Dong, Y. Gu, Y.-H. Chang, L. Zhang, L.-J. Li, W. Zhao, G. Eda, W. Zhang and G. Grinblat, Giant photoluminescence enhancement in tungsten-diselenide–gold plasmonic hybrid structures, *Nature Communications*, 7 (1) (2016) 11283.

[74] A. Banerjee, S.-U. H. Khan, S. Broadbent, R. Likhite, R. Looper, H. Kim and C. H. Mastrangelo, Batch-fabricated α-si assisted nanogap tunneling junctions, *Nanomaterials*, 9 (5) (2019) 727.

[75] V. Dubois, S. N. Raja, P. Gehring, S. Caneva, H. S. J. van der Zant, F. Niklaus and G. Stemme, Massively parallel fabrication of crack-defined gold break junctions featuring sub-3 nm gaps for molecular devices, *Nature Communications*, *9* (1) (2018) 3433.

[76] T. Ohshiro, K. Matsubara, M. Tsutsui, M. Furuhashi, M. Taniguchi and T. Kawai, Single-molecule electrical random resequencing of DNA and rna, *Scientific Reports*, 2 (1) (2012) 501.

[77] D. Bang, E.-J. Jo, S. Hong, J.-Y. Byun, J. Y. Lee, M.-G. Kim and L. P. Lee, Asymmetric nanocrescent antenna on upconversion nanocrystal, *Nano Letters*, 17 (11) (2017) 6583-6590.

[78] K. Santhosh, O. Bitton, L. Chuntonov and G. Haran, Vacuum rabi splitting in a plasmonic cavity at the single quantum emitter limit, *Nature Communications*, 7 (1) (2016) 11823.

[79] G. Zengin, G. Johansson, P. Johansson, T. J. Antosiewicz, M. Käll and T. Shegai, Approaching the strong coupling limit in single plasmonic nanorods interacting with j-aggregates, *Scientific Reports*, 3 (1) (2013) 3074.

[80] K.-D. Park, M. A. May, H. Leng, J. Wang, J. A. Kropp, T.

Gougousi, M. Pelton and M. B. Raschke, Tip-enhanced strong coupling spectroscopy, imaging, and control of a single quantum emitter, *Science Advances*, 5 (7) (2019) eaav5931.

[81] D. Ge, S. Marguet, A. Issa, S. Jradi, T. H. Nguyen, M. Nahra, J. Béal, R. Deturche, H. Chen, S. Blaize, J. Plain, C. Fiorini, L. Douillard, O. Soppera, X. Q. Dinh, C. Dang, X. Yang, T. Xu, B. Wei, X. W. Sun, C. Couteau and R. Bachelot, Hybrid plasmonic nano-emitters with controlled single quantum emitter positioning on the local excitation field, *Nature Communications*, 11 (1) (2020) 3414.

[82] S. J. Yoon, D. I. Song, J. Lee, M.-K. Kim, Y.-H. Lee and C.-K. Kim, Hopping of single nanoparticles trapped in a plasmonic double-well potential, *Nanophotonics*, 9 (16) (2020) 4729-4735.

[83] H. Cai, Q. Meng, H. Zhao, M. Li, Y. Dai, Y. Lin, H. Ding, N. Pan, Y. Tian, Y. Luo and X. Wang, High-throughput fabrication of ultradense annular nanogap arrays for plasmon-enhanced spectroscopy, *ACS Applied Materials & Interfaces*, 10 (23) (2018) 20189-20195.

[84] X. Chen, C. Ciraci, D. R. Smith and S. H. Oh, Nanogap-enhanced infrared spectroscopy with template-stripped wafer-scale arrays of buried plasmonic cavities, *Nano Letters*, 15 (1) (2015) 107-113.

[85] T. H. Le and T. Tanaka, Plasmonics–nanofluidics hydrid metamaterial: an ultrasensitive platform for infrared absorption spectroscopy and quantitative measurement of molecules, *ACS Nano*, 11 (10) (2017) 9780-9788.

[86] D. Yoo, D. A. Mohr, F. Vidal-Codina, A. John-Herpin, M. Jo, S. Kim, J. Matson, J. D. Caldwell, H. Jeon, N. C. Nguyen, L. Martin-Moreno, J. Peraire, H. Altug and S. H. Oh, High-contrast infrared absorption spectroscopy via mass-produced coaxial zero-mode resonators with sub-10 nm gaps, *Nano Letters*, 18 (3) (2018) 1930-1936.

[87] J. Mun, D. Lee, S. So, T. Badloe and J. Rho, Surface-enhanced spectroscopy: Toward practical analysis probe, *Applied Spectroscopy Reviews*, 54 (2) (2019) 142-175.

[88] S. So, M. Kim, D. Lee, D. M. Nguyen and J. Rho, Overcoming diffraction limit: From microscopy to nanoscopy, *Applied Spectroscopy Reviews*, 53 (2-4) (2018) 290-312.

[89] R. Huang, X. Ji, Y. Liao, J. Peng, K. Wang, Y. Xu and F. Yan, Dual-frequency cmos terahertz detector with silicon-based plasmonic antenna, *Optics Express*, 27 (16) (2019) 23250-23261.

[90] H.-R. Park, X. Chen, N.-C. Nguyen, J. Peraire and S.-H. Oh, Nanogap-enhanced terahertz sensing of 1 nm thick (λ/106) dielectric films, *ACS Photonics*, 2 (3) (2015) 417-424.

[91] A. Barik, X. Chen and S.H. Oh, Ultralow-power electronic trapping of nanoparticles with sub-10 nm gold nanogap electrodes, *Nano Letters*, 16 (10) (2016) 6317-6324.

[92] L. Lesser-Rojas, P. Ebbinghaus, G. Vasan, M.-L. Chu, A. Erbe and C.-F. Chou, Low-copy number protein detection by electrode nanogap-enabled dielectrophoretic trapping for surface-enhanced Raman spectroscopy and electronic measurements, *Nano Letters*, 14 (5) (2014) 2242-2250.

[93] M. Tsutsui, M. Taniguchi, K. Yokota and T. Kawai, Identifying single nucleotides by tunnelling current, *Nature Nanotechnology*, 5 (4) (2010) 286-290.

[94] W. Srituravanich, L. Pan, Y. Wang, C. Sun, D. B. Bogy and X. Zhang, Flying plasmonic lens in the near field for high-speed nanolithography, *Nature Nanotechnology*, 3 (12) (2008) 733-737.

[95] L. Pan, Y. Park, Y. Xiong, E. Ulin-Avila, Y. Wang, L. Zeng, S. Xiong, J. Rho, C. Sun and D.B. Bogy, Maskless plasmonic lithography at 22 nm resolution, *Scientific Reports*, 1 (1) (2011) 175.

[96] Y. Wang, Z. Du, Y. Park, C. Chen, X. Zhang and L. Pan, Quasi-3d plasmonic coupling scheme for near-field optical lithography and imaging, *Optics Letters*, 40 (16) (2015) 3918-3921.

[97] G. Yoon, I. Kim and J. Rho, Challenges in fabrication towards realization of practical metamaterials, *Microelectronic Engineering*, 163 (1) (2016) 7-20.

[98] N. Mahmood, I. Kim, M. Q. Mehmood, H. Jeong, A. Akbar, D. Lee, M. Saleem, M. Zubair, M. S. Anwar, F. A. Tahir and J. Rho, Polarisation insensitive multifunctional metasurfaces based on all-dielectric nanowaveguides, *Nanoscale*, 10 (38) (2018) 18323-18330.

[99] G. Yoon, D. Lee, K. T. Nam and J. Rho, Geometric metasurface enabling polarization independent beam splitting, *Scientific Reports*, 8 (1) (2018) 9468.

[100] N. Mahmood, H. Jeong, I. Kim, M. Q. Mehmood, M. Zubair, A. Akbar, M. Saleem, M. S. Anwar, F. A. Tahir and J. Rho, Twisted non-diffracting beams through all dielectric meta-axicons, *Nanoscale*, 11 (43) (2019) 20571-20578.

[101] G. Yoon, I. Kim, S. So, J. Mun, M. Kim and J. Rho, Fabrication of three-dimensional suspended, interlayered and hierarchical nanostructures by accuracy-improved electron beam lithography overlay, *Scientific Reports*, 7 (1) (2017) 6668.

[102] V. R. Manfrinato, F. E. Camino, A. Stein, L. Zhang, M. Lu, E. A. Stach and C. T. Black, Patterning si at the 1 nm length scale with aberration-corrected electron-beam lithography: Tuning of plasmonic properties by design, *Advanced Functional Materials*, 29 (52) (2019) 1903429.

[103] N. Pala and M. Karabiyik, *Electron Beam Lithography (ebl) for Encyclopedia of Nanotechnology*, Springer Netherlands, Dordrecht, Netherlands (2012).

[104] V. R. Manfrinato, A. Stein, L. Zhang, C.-Y. Nam, K. G. Yager, E. A. Stach and C. T. Black, Aberration-corrected electron beam lithography at the one nanometer length scale, *Nano Letters*, 17 (8) (2017) 4562-4567.

[105] V. R. Manfrinato, L. Zhang, D. Su, H. Duan, R. G. Hobbs, E. A. Stach and K. K. Berggren, Resolution limits of electron-beam lithography toward the atomic scale, *Nano Letters*, 13 (4) (2013) 1555-1558.

[106] H. Duan, H. Hu, K. Kumar, Z. Shen and J. K. W. Yang, Direct and reliable patterning of plasmonic nanostructures with sub-10-nm gaps, *ACS Nano*, 5 (9) (2011) 7593-7600.

[107] A. S. Gangnaik, Y. M. Georgiev, G. Collins and J. D. Holmes, Novel germanium surface modification for sub-10 nm patterning with electron beam lithography and hydrogen silsesquioxane resist, *J. of Vacuum Science & Technology B*, 34 (4) (2016)

041603.
[108] J. K. W. Yang, B. Cord, H. Duan, K. K. Berggren, J. Klingfus, S.-W. Nam, K.-B. Kim and M. J. Rooks, Understanding of hydrogen silsesquioxane electron resist for sub-5-nm-half-pitch lithography, *J. of Vacuum Science & Technology B*, 27 (6) (2009) 2622-2627.
[109] M. Manheller, S. Trellenkamp, R. Waser and S. Karthäuser, Reliable fabrication of 3 nm gaps between nanoelectrodes by electron-beam lithography, *Nanotechnology*, 23 (12) (2012) 125302.
[110] H. Duan, A. I. Fernández-Domínguez, M. Bosman, S. A. Maier and J. K. W. Yang, Nanoplasmonics: classical down to the nanometer scale, *Nano Letters*, 12 (3) (2012) 1683-1689.
[111] W. Zhu and K. B. Crozier, Quantum mechanical limit to plasmonic enhancement as observed by surface-enhanced raman scattering, *Nature Communications*, 5 (1) (2014) 5228.
[112] N. Arjmandi, L. Lagae and G. Borghs, Enhanced resolution of poly(methyl methacrylate) electron resist by thermal processing, *J. of Vacuum Science & Technology B*, 27 (4) (2009) 1915-1918.
[113] H. Duan, H. Hu, H. K. Hui, Z. Shen and J. K. W. Yang, Free-standing sub-10 nm nanostencils for the definition of gaps in plasmonic antennas, *Nanotechnology*, 24 (18) (2013) 185301.
[114] Y. Zhu, H. Inada, K. Nakamura and J. Wall, Imaging single atoms using secondary electrons with an aberration-corrected electron microscope, *Nature Materials*, 8 (10) (2009) 808-812.
[115] Y. Chen, Nanofabrication by electron beam lithography and its applications: A review, *Microelectronic Engineering*, 135 (1) (2015) 57-72.
[116] J. K. W. Yang and K. K. Berggren, Using high-contrast salty development of hydrogen silsesquioxane for sub-10-nm half-pitch lithography, *J. of Vacuum Science & Technology B*, 25 (6) (2007) 2025-2029.
[117] M. M. Mirza, H. Zhou, P. Velha, X. Li, K. E. Docherty, A. Samarelli, G. Ternent and D. J. Paul, Nanofabrication of high aspect ratio (~50:1) sub-10 nm silicon nanowires using inductively coupled plasma etching, *J. of Vacuum Science & Technology B*, 30 (6) (2012) 06FF02.
[118] M. Rommel, B. Nilsson, P. Jedrasik, V. Bonanni, A. Dmitriev and J. Weis, Sub-10 nm resolution after lift-off using hsq/pmma double layer resist, *Microelectronic Engineering*, 110 (1) (2013) 123-125.
[119] A. Vardi and J. A. d. Alamo, Sub-10-nm fin-width self-aligned ingaas finfets, *IEEE Electron Device Letters*, 37 (9) (2016) 1104-1107.
[120] K. Liu, P. Avouris, J. Bucchignano, R. Martel, S. Sun and J. Michl, Simple fabrication scheme for sub-10 nm electrode gaps using electron-beam lithography, *Applied Physics Letters*, 80 (5) (2002) 865-867.
[121] Y. Yang, C. Gu and J. Li, Sub-5 nm metal nanogaps: Physical properties, fabrication methods, and device applications, *Small*, 15 (5) (2019) 1804177.
[122] M. G. Stanford, B. B. Lewis, K. Mahady, J. D. Fowlkes and P. D. Rack, Review article: Advanced nanoscale patterning and material synthesis with gas field helium and neon ion beams, *J. of Vacuum Science & Technology B*, 35 (3) (2017) 030802.
[123] S. J. Yoon, J. Lee, S. Han, C.-K. Kim, C. W. Ahn, M.-K. Kim and Y.-H. Lee, Non-fluorescent nanoscopic monitoring of a single trapped nanoparticle via nonlinear point sources, *Nature Communications*, 9 (1) (2018) 2218.
[124] A. Cui, Z. Liu, H. Dong, Y. Wang, Y. Zhen, W. Li, J. Li, C. Gu and W. Hu, Single grain boundary break junction for suspended nanogap electrodes with gapwidth down to 1–2 nm by focused ion beam milling, *Advanced Materials*, 27 (19) (2015) 3002-3006.
[125] M. E. Schmidt, T. Iwasaki, M. Muruganathan, M. Haque, H. Van Ngoc, S. Ogawa and H. Mizuta, Structurally controlled large-area 10 nm pitch graphene nanomesh by focused helium ion beam milling, *ACS Applied Materials & Interfaces*, 10 (12) (2018) 10362-10368.
[126] R. Livengood, S. Tan, Y. Greenzweig, R. Hallstein, D. Shima, K. Klein and A. E. Vladar, A study of helium ion beam substrate interaction volume on nanomachining profiles in bulk substrates and thin film membranes, *Microscopy and Microanalysis*, 18 (S2) (2012) 808-809.
[127] M. M. Marshall, J. Yang and A. R. Hall, Direct and transmission milling of suspended silicon nitride membranes with a focused helium ion beam, *Scanning*, 34 (2) (2012) 101-106.
[128] S. Tan, K. Klein, D. Shima, R. Livengood, E. Mutunga and A. Vladár, Mechanism and applications of helium transmission milling in thin membranes, *J. of Vacuum Science & Technology B*, 32 (6) (2014) 06FA01.
[129] N. Kalhor, S. A. Boden and H. Mizuta, Sub-10nm patterning by focused he-ion beam milling for fabrication of downscaled graphene nano devices, *Microelectronic Engineering*, 114 (1) (2014) 70-77.
[130] M. G. Stanford, B. B. Lewis, V. Iberi, J. D. Fowlkes, S. Tan, R. Livengood and P. D. Rack, In situ mitigation of subsurface and peripheral focused ion beam damage via simultaneous pulsed laser heating, *Small*, 12 (13) (2016) 1779-1787.
[131] Y. Wang, M. Abb, S. A. Boden, J. Aizpurua, C. H. de Groot and O. L. Muskens, Ultrafast nonlinear control of progressively loaded, single plasmonic nanoantennas fabricated using helium ion milling, *Nano Letters*, 13 (11) (2013) 5647-5653.
[132] V. Sidorkin, E. van Veldhoven, E. van der Drift, P. Alkemade, H. Salemink and D. Maas, Sub-10-nm nanolithography with a scanning helium beam, *J. of Vacuum Science & Technology B*, 27 (4) (2009) L18-L20.
[133] X. Shi, P. Prewett, E. Huq, D. M. Bagnall, A. P. G. Robinson and S. A. Boden, Helium ion beam lithography on fullerene molecular resists for sub-10nm patterning, *Microelectronic Engineering*, 155 (1) (2016) 74-78.
[134] S. M. Lewis, M. S. Hunt, G. A. DeRose, H. R. Alty, J. Li, A. Wertheim, L. De Rose, G. A. Timco, A. Scherer, S. G. Yeates and R. E. P. Winpenny, Plasma-etched pattern transfer of sub-10 nm structures using a metal–organic resist and helium ion beam lithography, *Nano Letters*, 19 (9) (2019) 6043-6048.
[135] W.-D. Li, W. Wu and R. Stanley Williams, Combined helium ion beam and nanoimprint lithography attains 4 nm half-pitch dense patterns, *J. of Vacuum Science & Technology B*, 30 (6)

(2012) 06F304.

[136] S. Tan, R. Livengood, P. Hack, R. Hallstein, D. Shima, J. Notte and S. McVey, Nanomachining with a focused neon beam: A preliminary investigation for semiconductor circuit editing and failure analysis, *J. of Vacuum Science & Technology B*, 29 (6) (2011) 06F604.

[137] D. Xia, Y.-B. Jiang, J. Notte and D. Runt, Gaas milling with neon focused ion beam: Comparison with gallium focused ion beam milling and subsurface damage analysis, *Applied Surface Science*, 538 (1) (2021) 147922.

[138] R. W. Johnson, A. Hultqvist and S. F. Bent, A brief review of atomic layer deposition: from fundamentals to applications, *Materials Today*, 17 (5) (2014) 236-246.

[139] S. M. George, Atomic layer deposition: an overview, *Chemical Reviews*, 110 (1) (2010) 111-131.

[140] H. Im, K. C. Bantz, N. C. Lindquist, C. L. Haynes and S. H. Oh, Vertically oriented sub-10-nm plasmonic nanogap arrays, *Nano Letters*, 10 (6) (2010) 2231-2236.

[141] X. Chen, H. R. Park, M. Pelton, X. Piao, N. C. Lindquist, H. Im, Y. J. Kim, J. S. Ahn, K. J. Ahn, N. Park, D. S. Kim and S. H. Oh, Atomic layer lithography of wafer-scale nanogap arrays for extreme confinement of electromagnetic waves, *Nature Communications*, 4 (1) (2013) 2361.

[142] X. Chen, N. C. Lindquist, D. J. Klemme, P. Nagpal, D. J. Norris and S. H. Oh, Split-wedge antennas with sub-5 nm gaps for plasmonic nanofocusing, *Nano Letters*, 16 (12) (2016) 7849-7856.

[143] D. Yoo, N. C. Nguyen, L. Martin-Moreno, D. A. Mohr, S. Carretero-Palacios, J. Shaver, J. Peraire, T. W. Ebbesen and S. H. Oh, High-throughput fabrication of resonant metamaterials with ultrasmall coaxial apertures via atomic layer lithography, *Nano Letters*, 16 (3) (2016) 2040-2046.

[144] N. Kim, S. In, D. Lee, J. Rhie, J. Jeong, D.-S. Kim and N. Park, Colossal terahertz field enhancement using split-ring resonators with a sub-10 nm gap, *ACS Photonics*, 5 (2) (2017) 278-283.

[145] H. T. Miyazaki and Y. Kurokawa, Squeezing visible light waves into a 3-nm-thick and 55-nm-long plasmon cavity, *Physical Review Letters*, 96 (9) (2006) 097401.

[146] M. Kuttge, F. J. Garcia de Abajo and A. Polman, Ultrasmall mode volume plasmonic nanodisk resonators, *Nano Letters*, 10 (5) (2010) 1537-1541.

[147] Y. Q. Cao, K. Qin, L. Zhu, X. Qian, X. J. Zhang, D. Wu and A. D. Li, Atomic-layer-deposition assisted formation of wafer-scale double-layer metal nanoparticles with tunable nanogap for surface-enhanced raman scattering, *Scientific Reports*, 7 (1) (2017) 5161.

[148] S. Y. Chou, P. R. Krauss and P. J. Renstrom, Imprint of sub-25 nm vias and trenches in polymers, *Applied Physics Letters*, 67 (21) (1995) 3114-3116.

[149] C. Peroz, S. Dhuey, M. Cornet, M. Vogler, D. Olynick and S. Cabrini, Single digit nanofabrication by step-and-repeat nanoimprint lithography, *Nanotechnology*, 23 (1) (2012) 015305.

[150] J. Y. Woo, S. Jo, J. H. Oh, J. T. Kim and C. S. Han, Facile and precise fabrication of 10-nm nanostructures on soft and hard substrates, *Applied Surface Science*, 484 (1) (2019) 317-325.

[151] P. Gao, M. Pu, X. Ma, X. Li, Y. Guo, C. Wang, Z. Zhao and X. Luo, Plasmonic lithography for the fabrication of surface nanostructures with a feature size down to 9 nm, *Nanoscale*, 12 (4) (2020) 2415-2421.

[152] X. Zhang, X. Zhang, C. Luo, Z. Liu, Y. Chen, S. Dong, C. Jiang, S. Yang, F. Wang and X. Xiao, Volume-enhanced raman scattering detection of viruses, *Small*, 15 (11) (2019) 1805516.

[153] M. A. Verschuuren, M. W. Knight, M. Megens and A. Polman, Nanoscale spatial limitations of large-area substrate conformal imprint lithography, *Nanotechnology*, 30 (34) (2019) 345301.

[154] F. Hua, Y. G. Sun, A. Gaur, M. A. Meitl, L. Bilhaut, L. Rotkina, J. F. Wang, P. Geil, M. Shim, J. A. Rogers and A. Shim, Polymer imprint lithography with molecular-scale resolution, *Nano Letters*, 4 (12) (2004) 2467-2471.

[155] M. Nakagawa, A. Nakaya, Y. Hoshikawa, S. Ito, N. Hiroshiba and T. Kyotani, Size-dependent filling behavior of uv-curable di(meth)acrylate resins into carbon-coated anodic aluminum oxide pores of around 20 nm, *ACS Applied Materials & Interfaces*, 8 (44) (2016) 30628-30634.

[156] C. Pina-Hernandez, P. F. Fu and L. J. Guo, Ultrasmall structure fabrication via a facile size modification of nanoimprinted functional silsesquioxane features, *ACS Nano*, 5 (2) (2011) 923-931.

[157] S. Pi, P. Lin and Q. Xia, Fabrication of sub-10 nm metal nanowire arrays with sub-1 nm critical dimension control, *Nanotechnology*, 27 (46) (2016) 464004.

[158] H. Duan and K. K. Berggren, Directed self-assembly at the 10 nm scale by using capillary force-induced nanocohesion, *Nano Letters*, 10 (9) (2010) 3710-3716.

[159] H. Duan, J. K. Yang and K. K. Berggren, Controlled collapse of high-aspect-ratio nanostructures, *Small*, 7 (18) (2011) 2661-2668.

[160] C. Zhao, X. Xu, Q. Yang, T. Man, S. J. Jonas, J. J. Schwartz, A. M. Andrews and P. S. Weiss, Self-collapse lithography, *Nano Letters*, 17 (8) (2017) 5035-5042.

[161] Y. Xue, D. Kang, Y. Ma, X. Feng, J. A. Rogers and Y. Huang, Collapse of microfluidic channels/reservoirs in thin, soft epidermal devices, *Extreme Mechanics Letters*, 11 (1) (2017) 18-23.

[162] S. Gottlieb, M. Lorenzoni, L. Evangelio, M. Fernandez-Regulez, Y. K. Ryu, C. Rawlings, M. Spieser, A. W. Knoll and F. Perez-Murano, Thermal scanning probe lithography for the directed self-assembly of block copolymers, *Nanotechnology*, 28 (17) (2017) 175301.

[163] X. Y. Liu, M. Kumar, A. Calo, E. Albisetti, X. R. Zheng, K. B. Manning, E. Elacqua, M. Weck, R. V. Ulijn and E. Riedo, Sub-10 nm resolution patterning of pockets for enzyme immobilization with independent density and quasi-3d topography control, *ACS Applied Materials & Interfaces*, 11 (44) (2019) 41780-41790.

[164] H. Wolf, C. Rawlings, P. Mensch, J. L. Hedrick, D. J. Coady, U. Duerig and A. W. Knoll, Sub-20 nm silicon patterning and metal lift-off using thermal scanning probe lithography, *J. of Vacuum Science & Technology B*, 33 (2) (2014) 02B102.

[165] Y. K. R. Cho, C. D. Rawlings, H. Wolf, M. Spieser, S. Bisig, S. Reidt, M. Sousa, S. R. Khanal, T. D. B. Jacobs and A. W. Knoll, Sub-10 nanometer feature size in silicon using thermal scan-

ning probe lithography, *ACS Nano*, 11 (12) (2017) 11890-11897.

[166] W. B. Jung, S. Jang, S. Y. Cho, H. J. Jeon and H. T. Jung, Recent progress in simple and cost-effective top-down lithography for approximate to 10 nm scale nanopatterns: From edge lithography to secondary sputtering lithography, *Advanced Materials*, 32 (35) (2020) 1907101.

[167] H. J. Jeon, J. Y. Kim, W. B. Jung, H. S. Jeong, Y. H. Kim, D. O. Shin, S. J. Jeong, J. Shin, S. O. Kim and H. T. Jung, Complex high-aspect-ratio metal nanostructures by secondary sputtering combined with block copolymer self-assembly, *Advanced Materials*, 28 (38) (2016) 8439-8445.

[168] J. Baek, S. Y. Cho, H. Kang, H. Ahn, W. B. Jung, Y. Cho, E. Lee, S. W. Cho, H. T. Jung and S. G. Im, Distinct mechanosensing of human neural stem cells on extremely limited anisotropic cellular contact, *ACS Applied Materials & Interfaces*, 10 (40) (2018) 33891-33900.

[169] M. D. Austin, H. Ge, W. Wu, M. Li, Z. Yu, D. Wasserman, S. A. Lyon and S. Y. Chou, Fabrication of 5nm linewidth and 14nm pitch features by nanoimprint lithography, *Applied Physics Letters*, 84 (26) (2004) 5299-5301.

[170] B. Song, Y. Yao, R. E. Groenewald, Y. Wang, H. Liu, Y. Wang, Y. Li, F. Liu, S. B. Cronin, A. M. Schwartzberg, S. Cabrini, S. Haas and W. Wu, Probing gap plasmons down to subnanometer scales using collapsible nanofingers, *ACS Nano*, 11 (6) (2017) 5836-5843.

[171] F. Liu, B. Song, G. Su, O. Liang, P. Zhan, H. Wang, W. Wu, Y. Xie and Z. Wang, Sculpting extreme electromagnetic field enhancement in free space for molecule sensing, *Small*, 14 (33) (2018) 1801146.

[172] I. Kim, J. Mun, W. Hwang, Y. Yang and J. Rho, Capillary-force-induced collapse lithography for controlled plasmonic nanogap structures, *Microsystems & Nanoengineering*, 6 (1) (2020) 65.

[173] I. Kim, J. Mun, K. M. Baek, M. Kim, C. Hao, C.-W. Qiu, Y. S. Jung and J. Rho, Cascade domino lithography for extreme photon squeezing, *Materials Today*, 39 (1) (2020) 89-97.

[174] K. H. Nam, I. H. Park and S. H. Ko, Patterning by controlled cracking, *Nature*, 485 (7397) (2012) 221-224.

[175] V. Dubois, F. Niklaus and G. Stemme, Design and fabrication of crack-junctions, *Microsystems & Nanoengineering*, 3 (1) (2017) 17042.

[176] V. Dubois, F. Niklaus and G. Stemme, Crack-defined electronic nanogaps, *Advanced Materials*, 28 (11) (2016) 2178-2182.

[177] Q. Zhao, W. Wang, J. Shao, X. Li, H. Tian, L. Liu, X. Mei, Y. Ding and B. Lu, Nanoscale electrodes for flexible electronics by swelling controlled cracking, *Advanced Materials*, 28 (30) (2016) 6337-6344.

[178] Y. Chen, Q. Xiang, Z. Li, Y. Wang, Y. Meng and H. Duan, "Sketch and peel" lithography for high-resolution multiscale patterning, *Nano Letters*, 16 (5) (2016) 3253-3259.

[179] D. J. Beesley, J. Semple, L. Krishnan Jagadamma, A. Amassian, M. A. McLachlan, T. D. Anthopoulos and J. C. deMello, Sub-15-nm patterning of asymmetric metal electrodes and devices by adhesion lithography, *Nature Communications*, 5 (1) (2014) 3933.

[180] J. Semple, D. G. Georgiadou, G. Wyatt-Moon, M. Yoon, A. Seitkhan, E. Yengel, S. Rossbauer, F. Bottacchi, M. A. McLachlan, D. D. C. Bradley and T. D. Anthopoulos, Large-area plastic nanogap electronics enabled by adhesion lithography, *npj Flexible Electronics*, 2 (1) (2018) 18.

[181] T. W. Park, M. Byun, H. Jung, G. R. Lee, J. H. Park, H. I. Jang, J. W. Lee, S. H. Kwon, S. Hong, J. H. Lee, Y. S. Jung, K. H. Kim and W. I. Park, Thermally assisted nanotransfer printing with sub-20-nm resolution and 8-inch wafer scalability, *Science Advances*, 6 (31) (2020) eabb6462.

[182] W. Liu, Q. Zou, C. Zheng and C. Jin, Metal-assisted transfer strategy for construction of 2d and 3d nanostructures on an elastic substrate, *ACS Nano*, 13 (1) (2019) 440-448.

[183] Y. U. Lee, G. B. M. Wisna, S.-W. Hsu, J. Zhao, M. Lei, S. Li, A. R. Tao and Z. Liu, Imaging of nanoscale light confinement in plasmonic nanoantennas by brownian optical microscopy, *ACS Nano*, 14 (6) (2020) 7666-7672.

[184] M. Byun, D. Lee, M. Kim, Y. Kim, K. Kim, J. G. Ok, J. Rho and H. Lee, Demonstration of nanoimprinted hyperlens array for high-throughput sub-diffraction imaging, *Scientific Reports*, 7 (1) (2017) 46314.

[185] D. Lee, Y. D. Kim, M. Kim, S. So, H.-J. Choi, J. Mun, D. M. Nguyen, T. Badloe, J. G. Ok and K. Kim, Realization of wafer-scale hyperlens device for sub-diffractional biomolecular imaging, *ACS Photonics*, 5 (7) (2017) 2549-2554.

[186] J. Rho, Z. Ye, Y. Xiong, X. Yin, Z. Liu, H. Choi, G. Bartal and X. Zhang, Spherical hyperlens for two-dimensional sub-diffractional imaging at visible frequencies, *Nature Communications*, 1 (1) (2010) 143.

[187] S. So and J. Rho, Geometrically flat hyperlens designed by transformation optics, *J. of Physics D: Applied Physics*, 52 (19) (2019) 194003.

[188] M. A. May, D. Fialkow, T. Wu, K. D. Park, H. Leng, J. A. Kropp, T. Gougousi, P. Lalanne, M. Pelton and M. B. Raschke, Nano-cavity qed with tunable nano-tip interaction, *Advanced Quantum Technologies*, 3 (2) (2020) 1900087.

[189] X. Han, K. Wang, X. Xing, M. Wang and P. Lu, Rabi splitting in a plasmonic nanocavity coupled to a ws2 monolayer at room temperature, *ACS Photonics*, 5 (10) (2018) 3970-3976.

[190] M. Uemoto and H. Ajiki, Large and well-defined rabi splitting in a semiconductor nanogap cavity, *Optics Express*, 22 (19) (2014) 22470-22478.

[191] Y.-H. Hsieh, B.-W. Hsu, K.-N. Peng, K.-W. Lee, C. W. Chu, S.-W. Chang, H.-W. Lin, T.-J. Yen and Y.-J. Lu, Perovskite quantum dot lasing in a gap-plasmon nanocavity with ultralow threshold, *ACS Nano*, 14 (9) (2020) 11670-11676.

[192] J.-B. Kwon, S.-W. Kim, B.-H. Kang, S.-H. Yeom, W.-H. Lee, D.-H. Kwon, J.-S. Lee and S.-W. Kang, Air-stable and ultrasensitive solution-cast swir photodetectors utilizing modified core/shell colloidal quantum dots, *Nano Convergence*, 7 (1) (2020) 28.

[193] X. Yan and H. Wei, Strong plasmon–exciton coupling between lithographically defined single metal nanoparticles and monolayer wse 2, *Nanoscale*, 12 (17) (2020) 9708-9716.

[194] A. Das, K. Bae and W. Park, Enhancement of upconversion

luminescence using photonic nanostructures, *Nanophotonics*, 9 (6) (2020) 1359-1371.
[195] C. Gong, W. Liu, N. He, H. Dong, Y. Jin and S. He, Upconversion enhancement by a dual-resonance all-dielectric metasurface, *Nanoscale*, 11 (4) (2019) 1856-1862.
[196] C. Würth, P. Manley, R. Voigt, D. Ahiboz, C. Becker and U. Resch-Genger, Metasurface enhanced sensitized photon upconversion: toward highly efficient low power upconversion applications and nanoscale e-field sensors, *Nano Letters*, 20 (9) (2020) 6682-6689.
[197] S. Kim, H. Jung, Y. Kim, J. Jang and J. W. Hahn, Resolution limit in plasmonic lithography for practical applications beyond 2x-nm half pitch, *Advanced Materials*, 24 (44) (2012) OP337-OP344.
[198] A. Gee, A. H. Jaafar, B. Brachnakova, J. Massey, C. H. Marrows, I. Salitros and N. T. Kemp, Multilevel resistance switching and enhanced spin transition temperature in single and double molecule spin crossover nanogap devices, *The J. of Physical Chemistry C*, 124 (24) (2020) 13393-13399.
[199] X. Ji, K. Y. Pang and R. Zhao, Decoding the metallic bridging dynamics in nanogap atomic switches, *Nanoscale*, 11 (46) (2019) 22446-22455.
[200] Y.-W. Cho, J.-H. Park, K.-H. Lee, T. Lee, Z. Luo and T.-H. Kim, Recent advances in nanomaterial-modified electrical platforms for the detection of dopamine in living cells, *Nano Convergence*, 7 (1) (2020) 40.
[201] C. Jung, Y. Yang, J. Jang, T. Badloe, T. Lee, J. Mun, S.-W. Moon and J. Rho, Near-zero reflection of all-dielectric structural coloration enabling polarization-sensitive optical encryption with enhanced switchability, *Nanophotonics*, 10 (2) (2021) 919-926.
[202] G. Yoon, K. Kim, S.-U. Kim, S. Han, H. Lee and J. Rho, Printable nanocomposite metalens for high-contrast near-infrared imaging, *ACS Nano* (2021) (Article ASAP) DOI: doi.org/10.1021/acsnano.0c06968.

Dong Kyo Oh obtained his B.S. (2017) and M.S. (2019) in Mechanical and Automotive Engineering from Seoul National University of Science and Technology (SEOULTECH). Currently, he is a Ph.D. student in Mechanical Engineering at Pohang University of Science and Technology (POSTECH), Republic of Korea. His research is mainly focused on flat optics based on metasurfaces, nanofabrication of metamaterials, and alternative nanofabrication.

Joohoon Kim obtained his B.S. (2021) in Mechanical Engineering from POSTECH. Currently, he is an M.S./Ph.D. student in Mechanical Engineering at POSTECH. His research is mainly focused on nano-fabrication, metasurface holography, and active metasurfaces.

Heonyeong Jeong obtained his B.S. (2017) in Mechanical Engineering from POSTECH. Currently, he is a Ph.D. candidate in Mechanical Engineering at POSTECH. His research is mainly focused on nanofabrication, dielectric metasurfaces.

Yeseul Kim obtained her B.S. (2020) in Materials Science and Engineering from POSTECH. Currently, she is an M.S./Ph.D. student in Mechanical Engineering at POSTECH. Her research is mainly focused on topological photonics and flat optics based on metasurface.

Inki Kim obtained his B.S. (2015) in Mechanical Engineering from Ulsan National Institute of Science and Technology (UNIST) and Ph.D. (2021) in Mechanical Engineering at POSTECH. His research is mainly focused on metamaterials, metasurfaces, holograms, dynamic metasurfaces, and nanofabrication process.

Jong G. Ok is currently an Associate Professor of Mechanical and Automotive Engineering at SEOULTECH. He received his B.S. (2002) and M.S. (2007) in Mechanical and Aerospace Engineering at Seoul National University and Ph.D. (2013) in Mechanical Engineering at the University of Michigan, Ann Arbor. His research focuses on smart and scalable nanomanufacturing and multiscale hybrid nanoarchitecturing.

Junsuk Rho is currently a *Mu-En-Jae* endowed chair Associate Professor with a joint appointment in Mechanical Engineering and Chemical Engineering at POSTECH. His research is focused on developing novel nanophotonic materials and devices based on fundamental physics and experimental studies of deep sub-wavelength light-matter interaction. He received his B.S. (2007), M.S (2008), Ph.D. (2013) all in Mechanical Engineering at Seoul National University, University of Illinois, Urbana-Champaign, University of California, Berkeley, respectively.